

# Battery Degradation and Health Monitoring in Lithium-Ion Batteries: An Evaluation of Parameterization and Sensor Fusion Strategies

**Simon Saber**

Master of Science Thesis in Electrical Engineering  
**Battery Degradation and Health Monitoring in Lithium-Ion Batteries: An  
Evaluation of Parameterization and Sensor Fusion Strategies**

Simon Saber

LiTH-ISY-EX-24/5634-SE

Supervisor: **Fatemeh Hashemniya**  
ISY, Linköpings universitet

Examiner: **Daniel Jung**  
ISY, Linköpings universitet

*Division of Vehicular Systems  
Department of Electrical Engineering  
Linköping University  
SE-581 83 Linköping, Sweden*

Copyright © 2024 Simon Saber

## Abstract

The purpose of this project was to perform model-based diagnosis on Li-ion batteries using real-world data and sensor fusion algorithms. The data used in this project was collected and distributed by NASA and mainly consists of voltage and current measurements collected on numerous batteries that were repeatedly charged and discharged from their beginning of life, and until surpassing their end of life. The health of the batteries was decided by estimating their state of health through the increase in internal resistance. To validate the results, the increase in resistance was later compared with the decrease in charge capacity. Firstly an attempt was made to parameterize equivalent circuit models by fitting the model parameters to the data with a forgetting-factor recursive least squares filter, and a batch-wise recursive least squares filter. The forgetting factor recursive least squares filter proved unreliable and unable to consistently be able to parameterize the models. The batch-wise recursive least squares filter was able to consistently parameterize the models providing a root mean squared error of around 0.35V in simulated voltage response tests. In total 20 equivalent circuit models were parameterized for four batteries. The models were then used in conjunction with a standard Kalman filter and an unscented Kalman filter to further estimate the increase in internal resistance of the batteries throughout their lifetime. In addition, the state of charge of the batteries was tracked through Coulomb counting and later attempted to refine via the Kalman filters. The results were partly successful as both the standard and unscented Kalman filters were able to track the state of health of the batteries, albeit to a varying degree. However, the Kalman filters were unable to improve the state of charge estimation, thus highlighting a limitation in their application. While the Kalman filters showcased limitations in tracking the state of charge, their effectiveness in tracking the state of health thus proved that model-based approaches and sensor fusion algorithms can be utilized with both the standard Kalman filter and the unscented Kalman filter for meaningful health tracking.



## Acknowledgments

I want to extend my gratitude to my supervisor Ph.D. student Fatemeh Hashem-niya, whose expertise and guidance throughout this project have been instrumental in reaching the goals. Equally, I want to express my gratitude to my examiner Assoc. Prof. Daniel Jung, whose feedback and insightful criticism have helped deepen my knowledge and results.

*Linköping, February 2024*  
*Simon*



---

# Contents

<b>Notation</b>	<b>ix</b>
<b>1 Introduction</b>	<b>1</b>
1.1 Literature study . . . . .	1
1.2 Purpose and goal . . . . .	2
1.3 Problem formulation . . . . .	2
1.4 Research Questions . . . . .	3
1.5 Method . . . . .	3
<b>2 Theory</b>	<b>5</b>
2.1 Li-ion Battery Characteristics . . . . .	6
2.2 Li-ion Battery State Functions . . . . .	6
2.3 Li-ion battery modelling . . . . .	7
2.3.1 Electric-based models . . . . .	7
2.3.2 Thermal-based models . . . . .	8
2.3.3 Data-driven models . . . . .	8
2.4 State of health estimation . . . . .	8
2.5 State of charge estimation . . . . .	9
2.6 Fault Modes and Mechanisms . . . . .	9
<b>3 ECM Parameterization and SOH Estimation</b>	<b>11</b>
3.1 Dataset overview . . . . .	11
3.2 Outlier Rejection . . . . .	13
3.3 Batchwise Recursive Least Squares Filter . . . . .	14
3.4 Forgetting Factor Recursive Least Squares Filter . . . . .	16
3.5 Kalman Filter . . . . .	18
3.6 Unscented Kalman Filter . . . . .	20
<b>4 Results</b>	<b>23</b>
4.1 BRLS results . . . . .	24
4.2 FFRLS results . . . . .	26
4.3 Kalman filter results . . . . .	27
4.4 Unscented Kalman filter results . . . . .	28

---

4.5	State of health estimation . . . . .	29
<b>5</b>	<b>Discussion</b>	<b>33</b>
5.1	Limiting factors . . . . .	33
5.2	Parameterization Challenges . . . . .	34
5.3	Analyzing the performance of the Kalman filters . . . . .	36
5.4	Reflections on Study Aims . . . . .	40
<b>6</b>	<b>Conclusions and Future Work</b>	<b>43</b>
6.1	Conclusion . . . . .	43
6.2	Future work . . . . .	44
<b>7</b>	<b>Appendix</b>	<b>45</b>
7.1	Result from ECM parameterization and validation . . . . .	45
	<b>Bibliography</b>	<b>51</b>

---

# Notation

## ABBREVIATIONS

Abbreviation	Meaning
Li-ion	Lithium-ion
BOL	Beginning of life
EOL	End of life
ECM	Equivalent circuit model
OCV	Open circuit voltage
SOC	State of charge
SOH	State of health
RUL	Remaining useful life
BMS	Battery management system
FFRLS	Forgetting factor recursive least squares
BRLS	Batch-wise recursive least squares
KF	Kalman filter
UKF	Unscented Kalman filter
EKF	Extended Kalman filter
PF	Particle filter
RMSE	Root mean square error
ZOH	Zero-order hold
RC	Resistor capacitor
CV	Constant voltage
CC	Constant current
CCCV	Constant-current-constant-voltage



# 1

---

## Introduction

Lithium-ion (Li-ion) batteries can be found in many technical applications such as electric vehicles, smartphones, laptops, power tools, etc. As the world rallies to reduce its ecological footprint, the auto industry has begun a transition from fossil-fueled vehicles to electric alternatives, driven by both lawmakers and consumer demand. With this transition, the prevalence of Li-ion batteries is poised for substantial growth and this surge prompts new demands not only to comprehend but also to actively manage the ecological footprint of Li-ion batteries. One such aspect is being able to accurately track the health of a battery. Being able to better track battery health is important as degradation over time can result in a shortened life expectancy and potentially hazardous malfunction. Good health tracking is also vital for battery management systems (BMS) to effectively control and monitor the state of charge (SOC), thermal management, and charging management. Gaining insight into aging ultimately serves to cut costs for both manufacturers and consumers and limit the usage of the earth's resources.

### 1.1 Literature study

Li-ion battery health monitoring is an ongoing research field, where researchers worldwide are working to develop new ways to parameterize models and estimate state functions. For instance, Paris Ali Topan et al. [4] used recursive least squares to parameterize a model and a Kalman filter (KF) to estimate the SOC and the state of health (SOH). Datong Liu et al. instead used an unscented particle filter (UPF) to estimate the SOH. If a model-based approach is used, multiple ways of estimating the internal parameters of the model have been suggested in research. Rui Xiong et al. [5] used a particle filter (PF) to estimate the internal parameters of a Li-ion model and Jonghoon Kim and B. H. Cho [11] used an extended Kalman filter (EKF) to estimate the parameters. Another approach to

inner model parameter estimation was suggested by Ryan Ahmed et al. [6] where the parameters are estimated by using curve-fitting and optimization techniques to match model output with collected experimental discharge data.

The research field concerning modeling and health tracking of Li-ion batteries is only a subset of a larger research field concerning Li-ion batteries. For instance, one related field of study is that of fault isolation [8], which goes further than tracking the general health status of a battery. Here, one tries to discover the specific fault modes that give rise to degradation, so that adequate measures can be taken to restore the battery and/or improve them in the future. As Hu et al. [8] explain, this is no trivial task. The main data available to work with are temperature, current, and voltage, which tell little about the internal states of the battery. Thus there is a need for high fidelity models. Further on, it is a challenging task to deduce whether a faulty behavior stems from the battery, and not from the actuators, or the sensors.

Perhaps the closest field, which is highly linked to health tracking, is the development of battery management systems. The BMS is the central control unit managing and monitoring the battery. Since a battery in an electric vehicle consists of numerous smaller batteries, called cells, the BMS must ensure that temperature, voltage range, and current are held within the limits of the individual cell. Inputs to an effective BMS are common state functions like SOH and SOC

## 1.2 Purpose and goal

The purpose of this thesis is to study and evaluate methods for tracking the health of Li-ion batteries. The goal is to compile battery models suggested in research literature used for modeling and tracking battery degradation. Further on, a suitable model candidate will be identified and evaluated with the help of available experimental data. This will include how easy it is to parameterize the models with the available data, and how well these can be used in conjunction with sensor fusion algorithms such as extended Kalman filters (EKF) to keep track of degradation.

## 1.3 Problem formulation

The mentioned methods are just a sample of suggested approaches, and there are many more ways to approach this. What they all have in common is that they are trying to solve the underlying problem of tracking states that cannot directly be measured, but which are crucial to track to safely manage battery cells and extend their lifetime. Thus, it would be interesting to try and implement them, and later evaluate them in this thesis work. Comparing them in conjunction with experimental data could serve to investigate whether they are easy to implement, accurate, and/or computationally reasonable.

## 1.4 Research Questions

To relive the thesis work, some pre-made research questions have been prepared. These questions serve as a discussion point, to tie together the purpose with the results, and to spark further questions. More questions might arise along this tenure, and some might be dropped as more insight is gained. The following research questions are suggested.

1. What are the different types of battery models for diagnosis and how do they compare in purpose?
2. Are the implementation methods straightforward? If not, what are the reasons for complexity?
3. How do the models differ in terms of complexity and accuracy, and what are the challenges in model parametrization?

## 1.5 Method

To conduct this thesis work, suitable methods for both model parameterization and filtering for SOH estimation will be selected based on the literature study. The selected methods will then be examined by implementing them using real voltage and current data. Then a comparative analysis of the methods will be implemented by comparing the methods against each other, and also testing their robustness by testing the methods with data from different batteries. Finally, a discussion of the methods will be held regarding the research questions.



# 2

---

## Theory

In this chapter, the basic theory and characteristics of Li-ion batteries will be explained. Li-ion batteries are comprised of many components, and to understand how they work, some key components need to be understood. The Li-ion battery has a positive electrode, referred to as a cathode, and a negative electrode, referred to as an anode. The anode is made out of graphite and can store  $Li^+$  ions and electrons in its structure. The cathode can be made out of different lithium metal oxides, e.g. lithium cobalt oxide ( $LiCoO_2$ ) or lithium manganese oxide ( $LiMn_2O_4$ ), etc. These metal oxides contribute by offering a stable bond to lithium ions and electrons. Further on, there is an electrolyte between the cathode and anode which serves as a medium through which  $Li^+$  ions can pass, while not allowing electrons to pass through, thus preventing a short circuit between the electrodes.

During charging an external voltage is applied to the battery causing the anode to become negatively charged. This negative charge forces the  $Li^+$  ions to migrate to the anode due to electrostatic force. As  $Li^+$  ions migrate to the anode, the anode will gain a more positive charge, which in turn attracts electrons to move through the external circuit from the cathode to the anode. The battery is considered fully charged when enough  $Li^+$  ions and electrons have migrated to the anode, now intercalated in the graphite. During charging the potential of the electrodes will change, causing a voltage between the electrodes to build up. When discharging the battery (i.e. when using the battery) an external circuit connects the electrodes, going through the load, allowing electrons to migrate to the more positively charged cathode. The negative charge of the electrons will then start to attract  $Li^+$  ions, causing them to migrate back to the cathode where a stable bond is offered. When the lithium in the anode starts to get depleted the battery is considered fully discharged (i.e. empty), and the voltage between the electrodes will be depleted, albeit not at zero. One set of charging and discharg-

ing is called one battery cycle.

## 2.1 Li-ion Battery Characteristics

Many different parameters are used to characterize batteries. To understand the mechanism behind aging, some important characteristics of a Li-ion battery should be known. One such, is the battery's power capacitance, which is the maximum power the battery can deliver at any given moment, typically measured in watts (W). There is also the charge capacity, commonly only referred to as capacity, which is the amount of electric charge that can be stored, typically measured in ampere-hours (Ah). Another important characteristic is the internal impedance and internal resistance, measured in ohms ( $\Omega$ ). The internal resistance causes the greatest source of losses in Li-ion batteries, by directly opposing the current a battery produces. As a battery is a chemical storage unit, internal resistance is an umbrella term representing the cumulative effect of numerous resistances. These include ionic resistance from the electrolyte, electronic resistance in the electrode materials, and interface resistance between components [1]. Further on, open circuit voltage (OCV) is the voltage between the battery terminals when no current is flowing. The OCV is fundamental as it is included in many battery models, and is thus needed to estimate the SOH [3].

## 2.2 Li-ion Battery State Functions

The battery management system in e.g. electric vehicles relies on information about power and energy levels provided by state functions. These state functions are functions of other underlying parameters, as the name implies. These underlying parameters are not directly measurable and must be estimated via measured signals like current, temperature, and voltage [1].

One important state function is the state of charge. The SOC is a relationship between the available charge capacity and the total charge capacity, known as the nominal charge capacity. The relationship between the available capacity and the nominal capacity gives us a range of SOC from 1 to 0. Fully charged corresponds to 1, and fully discharged corresponds to 0. Theoretically, the SOC can be calculated by just integrating the current and dividing it by the total capacity. However, this builds up an error over time since you will integrate the measurement noise from the measured current.

Another important state function is the state of health, which indicates the current full charge capacity compared to the full charge capacity at the beginning of life (BOL). Estimating the SOH is a challenging task since the underlying degradation mechanisms are complex. Since the SOH is not a physical parameter, other relevant parameters need to be monitored, that can be used to represent the SOH. This could be the internal resistance, the impedance, the number of cycles, etc [1].

## 2.3 Li-ion battery modelling

Modeling plays an important role in health tracking and fault diagnosis of batteries. The models help estimate important health parameters such as state of health and remaining useful life (RUL). The different methods can either be physics-based mathematical models or data-driven models. Elmahallawy et al. [3] classify the models into four different categories. These are: electric-based models, thermal-based models, coupled thermal-electric models, and data-driven models. The first three categories are examples of the aforementioned physics-based mathematical models.

### 2.3.1 Electric-based models

The electric-based models can either be an equivalent circuit model (ECM) or an electrochemical model. An ECM is perhaps the most common electrical model and according to Hu et al. [8] the ECM approach is more commonly used in diagnostics as opposed to the electrochemical approach, as it is simpler in both structure and computation. The ECMs try to mimic the input-output characteristics by using electric circuit elements such as resistors, capacitors, and voltage sources in an open circuit. An illustration of a Thevenin model (a type of ECM) is shown in Figure 2.1. The resistor  $R_0$  represents the effect stemming from the internal resistance and the parallel resistor-capacitor represents the battery's ability to store and release charge and accounts for the non-linear behavior of the voltage profile.

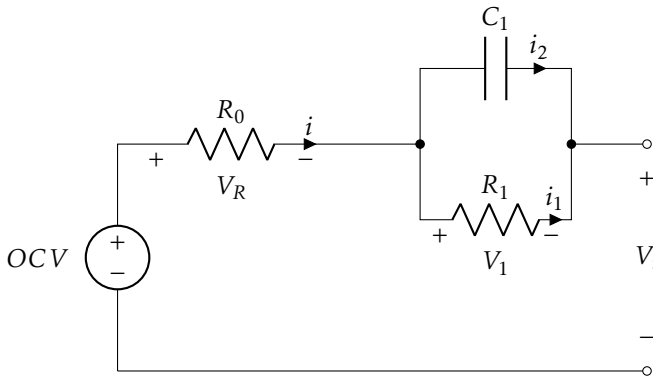


**Figure 2.1:** An illustration of a single RC-pair equivalent circuit model, called a Thevenin model.

The electrochemical model is the most accurate way of modeling Li-ion batteries, but also the most complex and computationally heavy. It involves differential equations that describe the electrochemical reaction within a cell. Due to the complexity of these models, full-order variants are not suitable for real-time applications. However, simplified reduced order variants can be used instead [3].

### 2.3.2 Thermal-based models

The thermal-based models work by modeling the generation, transfer, and distribution of heat inside the battery. These models can become very complex, depending on how accurate the models are, but generally, reduced order models are used in on-board applications [3]. A rather simple thermal model of the battery, from [9], could be set up as:

$$\dot{T} = \frac{I(OCV - V)}{mc} - \frac{hA}{mc}(T - T_{amb}), \quad (2.1)$$

where  $m$  is the mass of the battery,  $c$  is the specific heat capacity,  $A$  is the surface area,  $h$  is the convective heat transfer constant, and  $T_{amb}$  is the ambient temperature.

### 2.3.3 Data-driven models

The data-driven models treat the battery as a black box and thus only consider the relation between input signals (temperature, current, or voltage) and output signals (SOH, RUL) and try to find statistical correlations. This can be done by various machine learning algorithms such as state vector machines or artificial neural networks etc [3]. The data-driven models can also be purely based on signal processing, where feature extraction and enhancement methods can be used directly on the output signals to estimate the states of the battery [3].

## 2.4 State of health estimation

There are two common ways of calculating the SOH of a battery [3]. One way is by considering the change in charge capacity, where the battery has reached its end of life when the nominal capacity is 80% of the initial capacity. Another way to calculate the SOH is by considering the internal resistance of the battery. Here the internal resistance at the current moment is compared with internal resistance at the BOL. With this approach, the battery has reached its EOL when the internal resistance has doubled. Elmahallawy et al. [3] defines two main ways of estimating the SOH; these are by experimental methods and by model-based methods. The experimental methods involve storing parameter values and comparing them over time to estimate the SOH. However, these methods cannot be used in real-time applications and will thus not be considered. Further on, the model-based methods can be subdivided into adaptive filtering methods and data-driven methods. The adaptive filtering methods identify important external parameters and then use these with sensor fusion algorithms to estimate the SOH. The data-driven estimations use either data-fitting techniques or machine-learning algorithms to estimate the SOH with large amounts of collected data.

## 2.5 State of charge estimation

The common way to estimate the state of charge is via a method called Coulomb counting, shown below:

$$SOC(t) = SOC(t_0) + \frac{1}{C_{nom}} \int_{t_0}^t \eta i(\tau) d\tau. \quad (2.2)$$

This method works by continuously integrating the current as new measurements become available. Since the current is measured in ampere, which in turn is defined as charge per second, integrating the current thus renders in charge. So if the initial charge and the nominal capacity of the battery are known, it is theoretically possible to keep track of the state of charge in the battery. However, several flaws can make this method inaccurate. In Equation (2.2) the term  $\eta$ , which is the efficiency, can be seen included. This is to take into account energy losses occurring when charging and discharging. Further on, the measured current contains noise, which will also be integrated, thus corrupting the results, and determining the initial SOC can be difficult if the battery is not known to be either fully charged or fully discharged, and a bad initialization will cause severe inaccuracies. Another problem lies in determining the nominal capacity,  $C_{nom}$ , as this parameter will decrease throughout time and use due to degradation. Generally,  $C_{nom}$  can be determined through a discharge test where a fully charged battery is fully discharged, so the current passing through can be measured. Since temperature affects the chemical reactions in the battery, the SOC is temperature-dependent. Thus coulomb counting is a simplified method of SOC monitoring but with frequent re-initialization and good knowledge of the other parameters, the method is often sufficient.

To be able to estimate the SOC with discrete measurements, Equation (2.2) can be numerically approximated to look like the equation below:

$$SOC(k+1) = SOC(k) + \frac{\eta}{3600C_{nom}} \left( \frac{i(k+1) + i(k)}{2} \right) (t(k+1) - t(k)), \quad (2.3)$$

where  $k$  represents a discrete time step, and  $t(k)$  is the measured time at step  $k$ . The factor of 3600 is an optional conversion from Ah to As.

## 2.6 Fault Modes and Mechanisms

When discussing battery health, the expressions BOL, and EOL, are commonly used. This refers to the general health of the battery when it is newly made versus when the battery is old and should be replaced. The battery's real-time health is often compared with its health at BOL. The current health compared to the EOL indicates how long the battery will last. In general, the battery will start to degrade as soon as it is assembled and will continue to degrade whether is in use or not [1]. Therefore, a battery's lifetime can be measured in either calendar

time such as months and years, or in terms of the number of charge/discharge cycles. Both time measures are essential to keep in mind when working with batteries.

In the realm of diagnosis two important phrases often reoccur: fault modes and fault mechanisms. Fault mode refers to the specific way in which a fault might manifest itself. When working with batteries, two main features can be observed due to aging, these are capacity and power fade. Both mainly occur due to the loss of active material and cyclable lithium. In addition, a relatively higher temperature can be observed in a worn battery due to increased internal resistance.

When talking about fault mechanisms, one refers to the underlying mechanisms that give rise to faulty behavior. Li-ion batteries deteriorate due to several reasons, and the cause may be either mechanical or chemical in origin. Mechanical stress can come from vibration or shock from impacts, and they may cause structural damage to the current collectors situated on the electrodes, or damage the separator between the cathode and anode, etc [1]. Severe stress may cause a short circuit or a thermal runaway. A thermal runaway is in many regards the worst possible outcome, where chemical side reactions and gas buildup cause a chain reaction, which ultimately can ignite or explode the battery [8]. More moderate mechanical stress usually takes expression in the form of power and capacity fade [1]. Chemical fault mechanisms are complex by nature, but in summary, they are irreversible chemical reactions inside the cell. Some of the most significant mechanisms are the forming of the solid electrolyte interface (SEI), lithium plating (LP), and electrolyte decomposition which are chemical reactions that occur inside the cell. Electrolyte decomposition is a phenomenon when active materials in the electrolyte break down due to surrounding factors such as temperature and voltage [1], leading to reduced battery lifespan. The SEI is a layer that develops between the electrolyte and the anode when Li-ions react with the components in the decomposed electrolyte. Although the SEI ties up part of the Li-ion storage, it is an important safety feature by acting as an insulator preventing further electrolyte decomposition. Lithium plating is an undesirable phenomenon when Li-ions react with the graphite in the anode forming a layer on the surface of the anode, preventing Li-ions from intercalating in the graphite. These reactions tie up part of the lithium storage and active material in the electrolyte, leading to reduced capacity. Several factors contribute to these mechanisms, such as temperature, current rate, and state of charge [1].

# 3

---

## ECM Parameterization and SOH Estimation

In this section the methods used in the project will be described and derived. All the mentioned methods were implemented in MATLAB R2022b using the Control System Toolbox [12].

### 3.1 Dataset overview

As previously mentioned, the data used in this project is publicly available and provided by the Prognostics Center of Excellence (PCoE) at NASA. Finding good Li-ion battery data is a challenging task, and the data set provided by NASA is probably the most extensive provided within the field of Li-ion battery diagnostics. The data was collected over several years, and 36 batteries were continuously charged and discharged from their BOL and past their EOL. In addition, in between charge and discharge cycles, impedance measurements were carried out through electrochemical impedance spectroscopy sweeps from 0.1Hz to 5kHz. The batteries were commercially available Li-ion 18650-sized rechargeable batteries of an unspecified brand. They had a capacity of 2000mAh, a maximum voltage of 4.2V, and a cutoff voltage of 2.7V [2]. All batteries were charged under a constant-current-constant-voltage (CCCV) regimen, starting with a constant current (CC) of 1.5A until the voltage reached 4.2V, and then continuing in a constant voltage (CV) mode until the charge current dropped to 20mA. The discharging of the batteries was carried out under different regimens. Some approaches were to discharge the batteries with a constant current, or a wave current, amongst others. This project will focus specifically on batteries #5, #6, #7, and #18, which were charged under CCCV, and discharged with a 2A constant current until the voltage reached 2.7V, 2.5V, 2.2V, and 2.5V respectively. Since the cutoff voltage is 2.7V, the effect on aging caused by overuse can be studied.

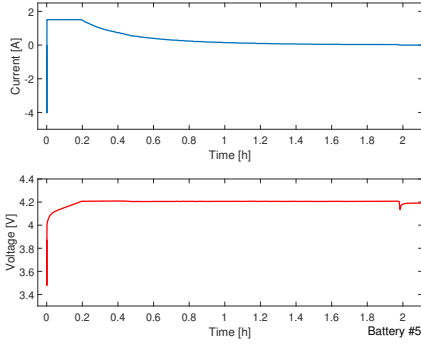


**Figure 3.1:** One charge cycle for battery #5.

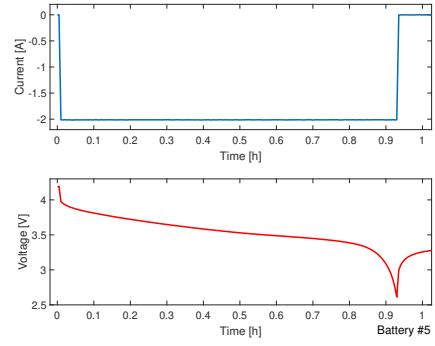


**Figure 3.2:** One discharge cycle for battery #5

In Figures 3.1 and 3.2 one charge and discharge cycle from battery #5 are shown. Furthermore, by studying the discharge cycles the adverse effects of aging can be identified. In Figure 3.3 the effects of aging are visible. As the battery capacity degrades due to loss in the active material, the discharge curve steadily moves to the left, meaning the battery discharges a bit quicker for each discharge.

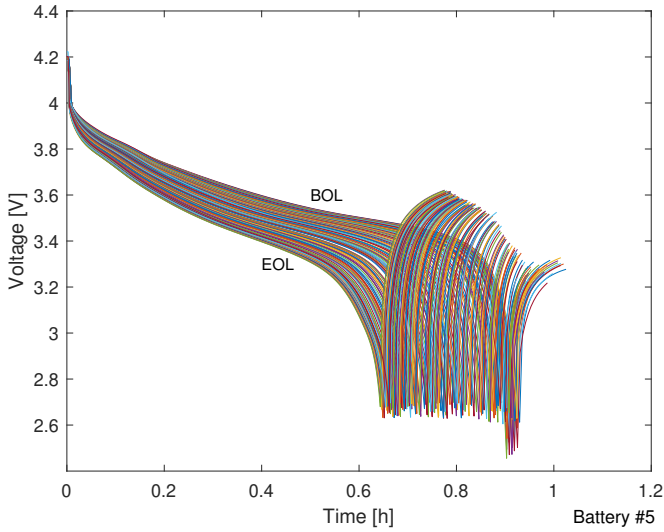


**Figure 3.3:** The voltage curve for all discharge cycles for battery #5 from BOL to EOL

Further on, the data contains measurement noise, of which the variance can be determined when the current and voltage are in their respective constant phases. In Figure 3.4 the effects of the measurement noise are shown. It can also be noted that a slight bias happens to be present, as the voltage should be at 4.2V, and the current at 1.5A. However, it can not be said whether this stems from sensor bias,

an actuator fault, or even the battery itself.

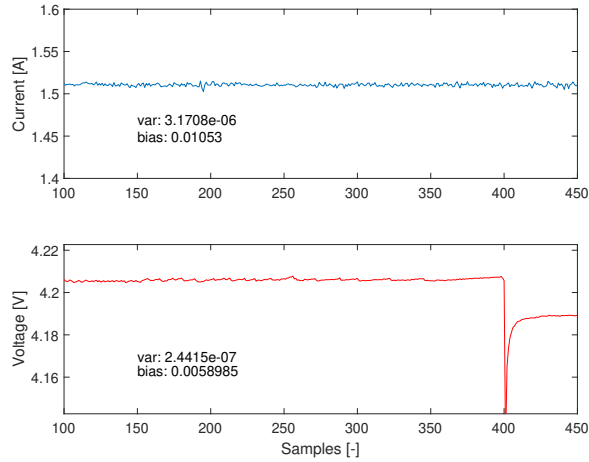


*Figure 3.4: Constant sections of current and voltage.*

## 3.2 Outlier Rejection

Looking at the raw data, some severe outlier measurements are visible. These likely do more harm than good in terms of numerical stability. Since they entail little knowledge about the state of degradation of the battery, it is prompt to have them removed. In this case, they were replaced by the previous acceptable measurement. This was done automatically through a simple algorithm that looks at each data point and replaces them if they surpass a certain threshold. The before and after from the outlier rejection can be seen in Figures 3.5 and 3.6.

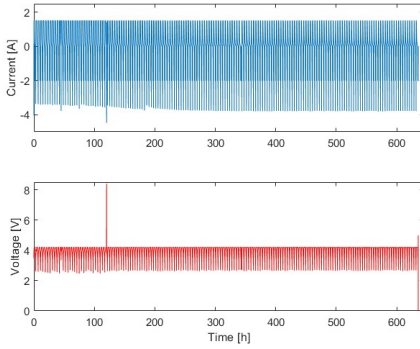


**Figure 3.5:** The raw current and voltage data from battery #5 pieced together with an artificial time vector representing the cycle time in calendar time.

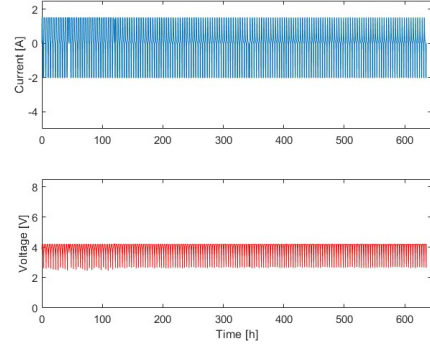


**Figure 3.6:** The processed current and voltage data from battery #5 pieced together with an artificial time vector representing the cycle time in calendar time.

### 3.3 Batchwise Recursive Least Squares Filter

Generally when an equivalent circuit model is parameterized, the available measurements to use are current, voltage, and temperature. More commonly though, only current and voltage are used, as including the temperature would require some kind of coupled thermal-electric model, thus increasing the model complexity. An issue with parameterizing an ECM is knowing the open circuit voltage, which is correlated to the SOC. Normally, the SOC will be estimated using Coulomb counting, and a pre-made look-up table will be used to interpolate a corresponding OCV value. However, if the OCV/SOC mapping is unknown, which is often the case, this approach will not be possible. Thus to resolve the problem of not knowing the OCV, a different approach is needed. In the paper [14] the authors present a method that circumvents this issue by instead considering the difference between consecutive measurements and omitting the OCV altogether. The assumption made is that with a small enough sampling time, the difference in OCV between consecutive measurements is negligible. Thus, the ECM parameters can be estimated without knowledge of the open circuit voltage, done with a recursive least squares filter, handling the data in batches.

The entire derivation of the model is lengthy, thus only a short derivation of the main equations is presented below, but for a full derivation see [14]. To begin, using Kirchhoff's voltage law, the Thevenin model can be described according to the following equation:

$$V_t(k) = OCV(k) + i(k)R_0 + i_1(k)R_1. \quad (3.1)$$

This equation can then be propagated one step forward in time:

$$V_t(k+1) = OC V(k+1) + i(k+1)R_0 + i_1(k+1)R_1, \quad (3.2)$$

and  $i_1(k+1)$  can be swapped for a discrete-time approximation according to:

$$i_1(k+1) = \alpha_1 i_1(k) + (1 - \alpha_1)i(k), \quad (3.3)$$

where

$$\alpha_1 = e^{\frac{-T_s}{R_1 C_1}}. \quad (3.4)$$

By subtracting the voltage equations from each other, assuming the difference in open circuit voltage equals zero, and then  $\mathcal{Z}$ -transforming it, eventually with algebraic manipulation, the equation can be put into matrix form according to:

$$V_t(k+1) - V_t(k) = \begin{bmatrix} V_t(k) - V_t(k-1) & i(k+1) - i(k) & -(i(k) - i(k-1)) \end{bmatrix} \begin{bmatrix} \alpha_1 \\ R_0 \\ \tilde{R}_1 \end{bmatrix} + \tilde{n}(k), \quad (3.5)$$

where  $\tilde{R}_1$  is a compound variable according to:

$$\tilde{R}_1 = \alpha_1 R_0 - (1 - \alpha_1)R_1. \quad (3.6)$$

The equation above can then be stacked by increasing  $k$ , and subsequently, the batch version can be written in the compact form, as shown below:

$$\tilde{\mathbf{V}}_k = \tilde{\mathbf{A}}_k \hat{\mathbf{b}} + \tilde{\mathbf{n}}_k, \quad (3.7)$$

where the index  $k$  now represents batch number. The uncertainty  $\tilde{\mathbf{n}}_k$  has a covariance matrix according to:

$$\Sigma_k = \begin{bmatrix} \sigma_n^2(0) & \sigma_n^2(1) & & & \\ \sigma_n^2(1) & \sigma_n^2(0) & \sigma_n^2(1) & & \\ & \ddots & \ddots & \ddots & \\ & & \sigma_n^2(1) & \sigma_n^2(0) & \sigma_n^2(1) \\ & & & \sigma_n^2(1) & \sigma_n^2(0) \end{bmatrix}, \quad (3.8)$$

where  $\Sigma_k$  is a square matrix with the same dimension as the size of the batch, and all unspecified elements are set to zero. The variance and covariance  $\sigma_n^2(1)$  and  $\sigma_n^2(0)$  are defined according to:

$$\begin{cases} \sigma_n^2(0) = 2(1 + \alpha_1^2)\sigma_v^2 + 2(R_0^2 + \tilde{R}_1^2)\sigma_i^2, \\ \sigma_n^2(1) = -2\alpha_1\sigma_v^2 - 2R_0\tilde{R}_1\sigma_i^2, \end{cases} \quad (3.9)$$

where  $\sigma_i^2$  and  $\sigma_v^2$  are the variance of the noise for the current and voltage measurements respectively. With all of the above defined, the filter can be initialized and run according to the recursions in Algorithm (1). The estimates  $\hat{\mathbf{b}}$  can then be converted back to ECM parameters using the following conversion:

$$\begin{cases} R_0 = \hat{b}(2) \\ R_1 = \frac{\hat{b}(1)\hat{b}(2)}{1-\hat{b}(1)} \\ C_1 = \frac{T_s}{R_1 \ln(\hat{b}(1))} \end{cases} \quad (3.10)$$

---

**Algorithm 1** Batchwise Recursive Least Squares Algorithm

Initialize with  $\hat{b}_1 = (\tilde{\mathbf{A}}_1^T \tilde{\mathbf{A}}_1)^{-1} \tilde{\mathbf{A}}_1^T \tilde{\mathbf{V}}_1$  and  $P_1 = (\tilde{\mathbf{A}}_1^T \tilde{\mathbf{A}}_1)^{-1}$

---

- 1: Construct the noise covariance matrix  $\Sigma_k$  using Equation (3.8)
  - 2: Update Error Covariance:  $P_{k+1}^{-1} = P_k^{-1} - \tilde{\mathbf{A}}_{k+1}^T \Sigma_k^{-1} \tilde{\mathbf{A}}_{k+1}$
  - 3: Update Residual Covariance:  $S_{k+1} = \tilde{\mathbf{A}}_{k+1} P_{k+1}^{-1} \tilde{\mathbf{A}}_{k+1}^T + \Sigma_k$
  - 4: Update gain:  $K_{k+1} = P_{k+1} \tilde{\mathbf{A}}_{k+1}^T S_{k+1}^{-1}$
  - 5: Update Estimates:  $\hat{b}_{k+1} = \hat{b}_k + K_{k+1}(\tilde{\mathbf{V}}_{k+1} - \tilde{\mathbf{A}}_{k+1} \hat{b}_k)$
- 

### 3.4 Forgetting Factor Recursive Least Squares Filter

Another approach to parameterizing an ECM is by using a forgetting factor recursive least squares method. This method is utilized in [7], and it differs from the BRLS filter in that it does utilize an OCV-SOC mapping. The mapping is borrowed from [13] and is derived for a Li-ion battery with similar voltage specs. The mapping can be seen in Figure 3.7. Below, a brief derivation of the method will follow, but for more detail see the original paper [7]. To begin with, the single RC-pair ECM in Figure 2.1 is again chosen as a model. The relationship between the current going through the circuit, and the current going through the RC-pair, can be described with Kirchhoff's current law according to:

$$i(t) = i_1(t) + i_2(t). \quad (3.11)$$

Further on, the relationship between the current going through the capacitor and the voltage over said component is  $i_2(t) = C_1 \dot{V}_1(t)$ . The current going through the resistor in the RC-pair, can with Ohm's law be replaced with  $i_1(t) = \frac{V_1(t)}{R_1}$ . With both of these relationships (3.11) can be rewritten into the following:

$$\dot{V}_1(t) = -\frac{V_1(t)}{R_1 C_1} + \frac{i(t)}{C_1}. \quad (3.12)$$

This equation can then be Laplace transformed so that the transfer function,  $G(s) : I(s) \rightarrow V_1(s)$  can be derived:

$$V_1(s) = I(s) \frac{R_1}{1 + sR_1 C_1}. \quad (3.13)$$

Moving on, with Kirchhoff's voltage law, the relationships between the components in the circuit can be described according to:

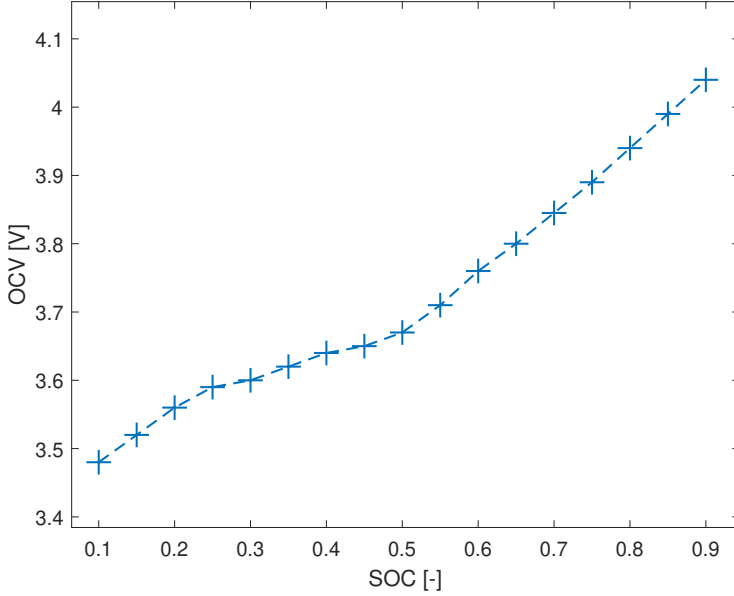


**Figure 3.7:** OCV-SOC curve interpolated from visually interpreted values provided by CALCE at the University of Maryland [13].

$$V_t(t) = OCV(t) - i(t)R_0 - V_1(t). \quad (3.14)$$

The equation above is then  $\mathcal{L}$ -transformed, and subsequently  $V_1(s)$  can be replaced with Equation (3.13) to form:

$$\begin{aligned} V_t(s) &= OCV(s) - I(s)R_0 - I(s)\frac{R_1}{1 + sR_1C_1} \Leftrightarrow, \\ V_t(s) - OCV(s) &= -I(s) \underbrace{\left( R_0 + \frac{R_1}{1 + sR_1C_1} \right)}_{H(s): I(s) \rightarrow V_t(s) - OCV(s)}. \end{aligned} \quad (3.15)$$

The equation above can now be  $\mathcal{Z}$ -transformed using bilinear transformation where  $s = \frac{2}{T_s} \frac{1-z^{-1}}{1+z^{-1}}$  and the transfer function  $H(s)$  can be substituted with with a parameterized transfer function,  $H_1(z) = \frac{c_2 + c_3 z^{-1}}{1 + c_1 z^{-1}}$  so that the least squares problem is solved for  $c_1$ ,  $c_2$ , and  $c_3$ . The estimates can then be converted back to ECM parameters with the following conversion:

$$\begin{cases} R_1 = \frac{2(c_1 c_2 - c_3)}{c_1^2 - 1}, \\ C_1 = \frac{-T(c_1 - 1)^2}{4(c_1 c_2 - c_3)}, \\ R_0 = \frac{c_3 - c_2}{c_1 - 1}. \end{cases} \quad (3.16)$$

Finally, the expression can be written in matrix form, where  $k$  represents a discrete time step:

$$V_t(k) - OCV(k) = \begin{bmatrix} V_t(k-1) - OCV(k-1) & i(k) & i(k-1) \end{bmatrix} \begin{bmatrix} c_1 \\ c_2 \\ c_3 \end{bmatrix}. \quad (3.17)$$

This can then be written in auto-regressive exogenous (ARX) form:

$$y_k = \varphi_k \theta_k. \quad (3.18)$$

To derive the OCV(k) component, in parallel with the filter a Coulomb count will be performed according to (2.3) and for each new SOC value, an OCV value will be interpolated from the mapping in Figure 3.7. Finally, the filter can be initialized and run according to the recursions of Algorithm (2).

---

**Algorithm 2** Forgetting Factor Recursive Least Squares Algorithm

---

Initialize with  $\hat{\theta}_1 = (\varphi_1^T \varphi_1)^{-1} \varphi_1^T y_1$  and  $P_1 = (\varphi_1^T \varphi_1)^{-1}$  and  $0 < \lambda < 1$

---

- 1: Calculate gain:  $K_k = \frac{P_{k-1} \varphi_k^T}{\varphi_k P_{k-1} \varphi_k^T + \lambda}$
  - 2: Update error covariance matrix:  $P_k = \frac{P_{k-1} - K_k \varphi_k^T P_{k-1}}{\lambda}$
  - 3: Calculate prediction error:  $e_k = y_k - \varphi_k \hat{\theta}_{k-1}$
  - 4: Update estimate:  $\hat{\theta}_k = \hat{\theta}_{k-1} + K_k e_k$
- 

### 3.5 Kalman Filter

Once an equivalent circuit model has been parameterized, the model can be used in conjunction with a Kalman filter to try and gain better estimates for the internal resistance, which could lead to better SOH estimates. The method presented below was introduced in [4] and attempts to estimate SOC, internal resistance, and the RC voltage. To derive the model equations, the process begins with deriving the equation that describes how the voltage across the resistor-capacitor pair changes over time, given the model parameters and current:

$$\dot{V}_1(t) = -\frac{V_1(t)}{R_1 C_1} + \frac{i(t)}{C_1}. \quad (3.19)$$

This equation can now be identified as an ordinary differential equation which has an analytical solution according to:

$$V_1(t) = e^{\frac{-(t-t_0)}{R_1 C_1}} V_1(t_0) + \int_{t_0}^t e^{\frac{-(t-\tau)}{R_1 C_1}} \frac{1}{C_1} i(\tau) d\tau. \quad (3.20)$$

The expression can then be further developed by solving the integral while treating the current as a constant, as it can be regarded as a constant parameter that changes at different time steps, as opposed to a variable that changes over time:

$$\begin{aligned}
 V_1(t) &= e^{\frac{-(t-t_0)}{R_1 C_1}} V_1(t_0) + \frac{i}{C_1} \left[ \frac{e^{\frac{-(t-\tau)}{R_1 C_1}}}{\frac{1}{R_1 C_1}} \right]_{t_0}^t \\
 &= e^{\frac{-(t-t_0)}{R_1 C_1}} V_1(t_0) + \frac{i R_1 C_1}{C_1} \left[ e^{\frac{-(t-t)}{R_1 C_1}} - e^{\frac{-(t-t_0)}{R_1 C_1}} \right] \\
 &= e^{\frac{-(t-t_0)}{R_1 C_1}} V_1(t_0) + i R_1 \left( 1 - e^{\frac{-(t-t_0)}{R_1 C_1}} \right).
 \end{aligned} \tag{3.21}$$

The last expression can now be treated as a time-discrete equation by substituting  $t$  for  $k + 1$  and  $t_0$  for  $k$ , whilst treating  $t - t_0$  as the sampling time  $T_s$ . This gives a final time-discrete expression for the voltage change:

$$V_1(k + 1) = e^{\frac{-T_s}{R_1 C_1}} V_1(k) + R_1 \left( 1 - e^{\frac{-T_s}{R_1 C_1}} \right) I(k). \tag{3.22}$$

Further on, an expression for the SOC is needed, and here a zero-order hold (ZOH) version of (2.3) is used:

$$SOC(k + 1) = SOC(k) + \frac{\eta I(k) T_s}{3600 C_{nom}} \tag{3.23}$$

Finally, these equations can be used in conjunction with the ECM voltage relationship, described in (3.14), to form the model equations in the Kalman filter:

$$x(k + 1) = \begin{bmatrix} 1 & 0 & 0 & \frac{\eta T_s I(k)}{3600} & 0 \\ 0 & e^{\frac{-T_s}{R_1 C_1}} & 0 & 0 & 0 \\ 0 & 0 & 1 & 0 & 0 \\ 0 & 0 & 0 & 1 & 0 \\ 0 & 0 & 0 & C_{cap} & 0 \end{bmatrix} \begin{bmatrix} SOC \\ V_1 \\ R_0 \\ \frac{1}{C_{nom}} \\ SOH \end{bmatrix} + \begin{bmatrix} 0 \\ R_1 (1 - e^{\frac{-T_s}{R_1 C_1}}) \\ 0 \\ 0 \\ 0 \end{bmatrix} I(k), \tag{3.24}$$

$$y(k) = \begin{bmatrix} \frac{dOCV}{dSOC} & -1 & I(k) & 0 & 0 \end{bmatrix} \begin{bmatrix} SOC \\ V_1 \\ R_0 \\ \frac{1}{C_{nom}} \\ SOH \end{bmatrix}. \tag{3.25}$$

These can then be written in compact form, now with the time index in subscripts for easier notation:

$$x_{k+1} = A_k x_k + B_k I_k + v, \tag{3.26}$$

$$y_k = C_k x_k + e, \tag{3.27}$$

where  $v$  and  $e$  represent the variance of the process and measurement noise modeled as  $q \sim \mathcal{N}(0, v)$  and  $R \sim \mathcal{N}(0, e)$ , the Kalman filter can now be run using the standard Kalman recursions shown in Algorithm (3), while using measured voltage as  $y_k$ . In addition, parallel with the Kalman filter, a numerical Coulomb counting is performed to update the measurement model matrix  $C_k$ . Again, the pre-made OCV-SOC look-up table available at [13] is used to interpolate OCV values based on the calculated SOC value, and subsequently, numerical integration is performed to derive the  $\frac{dOCV}{dSOC}$ .

---

**Algorithm 3** Kalman Filter

Initialize with  $\hat{x}_{0|0}$ ,  $P_{0|0}$ ,  $R$ ,  $q$

---

- 1: Propagate estimate:  $\hat{x}_{k+1|k} = A_k \hat{x}_{k|k} + B_k I_k$
  - 2: Update uncertainty:  $P_{k+1|k} = A_k P_{k|k} A_k^T + q q^T$
  - 3: Calculate innovation:  $\varepsilon_k = y_k - C_k \hat{x}_{k+1|k}$
  - 4: Calculate innovation covariance:  $S_k = C_k P_{k+1|k} C_k^T + R_k$
  - 5: Calculate Kalman gain:  $K_k = P_{k+1|k} C_k^T (C_k P_{k+1|k} C_k^T + R_k)^{-1}$
  - 6: Measurement update estimate:  $\hat{x}_{k+1|k+1} = \hat{x}_{k+1|k} + K_k \varepsilon_k$
  - 7: Measurement update uncertainty:  $P_{k+1|k+1} = P_{k+1|k} - K_k S_k K_k^T$
- 

### 3.6 Unscented Kalman Filter

Another Kalman filter technique is the unscented Kalman filter, which is built to handle nonlinearities better. The filter works differently from the regular Kalman recursions. Instead of propagating the estimates, it generates several sigma points based on the probability distribution of the model and instead propagates these sigma points. The measurement update works by estimating the measurement with the sigma points and then comparing it to the actual measurement. The following method was inspired by. [7]. The unscented Kalman filter uses slightly different model equations compared to the Kalman filter. The SOH and  $C_{nom}$  states are dropped and instead, the knowledge is compounded in the model matrices. The model takes on the following form:

$$x_{k+1} = \begin{bmatrix} 1 & 0 & 0 \\ 0 & 1 & 0 \\ 0 & 0 & e^{\frac{-T_s}{R_1 C_1}} \end{bmatrix} x_k + \begin{bmatrix} \frac{\eta T_s}{3600 C_{nom}} \\ 0 \\ R_1 (1 - e^{\frac{-T_s}{R_1 C_1}}) \end{bmatrix} I_k, \quad (3.28)$$

$$\Leftrightarrow x_{k+1} = A_k x_k + B_k I_k, \quad (3.29)$$

where  $x_k = [SOC, R_0, V_1]^T$ . And similar to the KF the measurement update is described according to:

$$y_k = \begin{bmatrix} \frac{dOCV}{dSOC} & -1 & I_k \end{bmatrix} x_k, \quad (3.30)$$

$$\Leftrightarrow y_k = C_k x_k. \quad (3.31)$$

To begin, the states that need estimation are modeled as a Gaussian distribution  $x \sim \mathcal{N}(\mu_x, P)$ , where the mean  $\mu_x$  in this case is the initial state, and covariance  $P$  the initial uncertainty. Based on  $P$ , a singular value decomposition is performed according to  $P = U\Sigma U^T$ . Now  $2n_x + 1$  sigma points are created, where  $n_x$  is the dimension of the state vector  $x$ , so in this case there is a total of seven sigma points. The sigma points are generated according to:

$$x_{k|k}^{(0)} = \mu_x, \quad (3.32)$$

$$x_{k|k}^{(\pm i)} = \mu_x \pm \sqrt{n_x + \lambda} \sigma_i u_i. \quad (3.33)$$

Where  $i = 1, \dots, n_x$ , and  $\sigma_i$  is the  $i$ :th diagonal element in  $\Sigma$ , and  $u_i$  is the  $i$ :th column in  $U$ . The corresponding weights given to each sigma point are calculated according to:

$$\omega^{(0)} = \frac{\lambda}{n_x + \lambda}, \quad (3.34)$$

$$\omega^{(\pm i)} = \frac{1}{2(n_x + \lambda)}. \quad (3.35)$$

The UKF has three extra tuning parameters,  $\alpha$ ,  $\beta$ , and  $\kappa$ . The  $\alpha$  parameter controls the spread of the sigma points around the mean and is usually set to approximately 0.001 [10].  $\beta$  is used to compensate for the distribution of the state and is set to 2 for Gaussian distributions [10]. Lastly,  $\kappa$  is a secondary scaling parameter used to adjust the mean of the sigma points, which is  $x^{(0)}$ . However,  $\kappa$  is usually set to zero [10].  $\lambda$  is a design parameter defined by the previously explained parameters as  $\lambda = \alpha^2(n_x + \kappa) - n_x$ . To perform the time update, the sigma points are first propagated through the model equation:

$$x_{k+1|k}^{(\pm i)} = A_k x_{k|k}^{(\pm i)} + B_k I_k. \quad (3.36)$$

Then the predicted states and predicted covariance matrix are calculated with the help of the propagated sigma points and the corresponding weights:

$$\hat{x}_{k+1|k} = \sum_{i=-n_x}^{n_x} \omega^{(i)} x_{k+1|k}^{(i)}, \quad (3.37)$$

$$P_{k+1|k}^{xx} = \sum_{i=-n_x}^{n_x} \omega^{(i)} (x_{k+1|k}^{(i)} - \hat{x}_{k+1|k})(x_{k+1|k}^{(i)} - \hat{x}_{k+1|k})^T + Q, \quad (3.38)$$

where  $Q$  is the process noise. To perform the measurement update, the propagated sigma points are mapped onto the measurement space through the measurement equation:

$$y_{k+1|k}^{(i)} = C_k x_{k+1|k}^{(i)}. \quad (3.39)$$

Then the distribution of the measurements is modeled as  $y^{(i)} \sim \mathcal{N}(\hat{y}, P^{yy})$ , where  $\hat{y}$  and  $P^{yy}$  are calculated with the help of the weights and the previously calculated measurements  $y_{k+1|k}^{(i)}$ :

$$\hat{y}_{k+1|k} = \sum_{i=-n_x}^{n_x} \omega^{(i)} y_{k+1|k}^{(i)}, \quad (3.40)$$

$$P_{k+1|k}^{yy} = \sum_{i=-n_x}^{n_x} \omega^{(i)} (y_{k+1|k}^{(i)} - \hat{y}_{k+1|k}) (y_{k+1|k}^{(i)} - \hat{y}_{k+1|k})^T + (1 - \alpha^2 + \beta) (y_{k+1|k}^{(0)} - \hat{y}_{k+1|k}) (y_{k+1|k}^{(0)} - \hat{y}_{k+1|k})^T. \quad (3.41)$$

Now that the distribution for both the predicted states and the predicted measurements has been determined, a new joint distribution between the states and the measurement can be modeled as:

$$\mathcal{Z} = \begin{pmatrix} x_{k+1|k} \\ y_{k+1|k} \end{pmatrix} \sim \mathcal{N} \left( \begin{pmatrix} \hat{x}_{k+1|k} \\ \hat{y}_{k+1|k} \end{pmatrix}, \begin{pmatrix} P_{k+1|k}^{xx} & P_{k+1|k}^{xy} \\ P_{k+1|k}^{yx} & P_{k+1|k}^{yy} \end{pmatrix} \right), \quad (3.42)$$

where the cross-covariance  $P_{k+1|k}^{yx} = P_{k+1|k}^{xy}$  can be calculated as:

$$P_{k+1|k}^{xy} = \sum_{i=-n_x}^{n_x} (x_{k+1|k}^{(i)} - \hat{x}_{k+1|k}) (y_{k+1|k}^{(i)} - \hat{y}_{k+1|k})^T. \quad (3.43)$$

At last, the Kalman gain can be calculated, and the measurement update finished:

$$K_{k+1} = P_{k+1|k}^{xy} (P_{k+1|k}^{yy})^{-1}, \quad (3.44)$$

$$\hat{x}_{k+1|k+1} = \hat{x}_{k+1|k} + K_{k+1} (y_{k+1} - \hat{y}_{k+1|k}), \quad (3.45)$$

$$P_{k+1|k+1} = P_{k+1|k}^{xx} - K_{k+1} P_{k+1|k}^{yy} K_{k+1}^T. \quad (3.46)$$

# 4

---

## Results

This section presents the results from the methods previously described. Given the large amount of data, using all data when parameterizing the ECM or running a Kalman filters was not feasible. Since there were multiple batteries, and each battery had been measured for around two months, an intelligent selection had to be made. The subset of data from each battery used in this project was consistently chosen in five intervals. Depending on the algorithm and how much data was needed for the results to converge, the number of cycles per interval can vary from one or three cycles for the forgetting factor recursive least squares filter, or as much as 20 cycles for the batch-wise recursive least squares filter. The intervals were chosen at roughly equal distances in terms of calendar time, as to be able to capture the degradation over time. The first interval was reasonably chosen at the BOL, and the last interval was reasonably chosen at the EOL. Then the remaining three intervals were chosen in between those. Further on, since the data collection had taken course over a considerable amount of time, the measured cycles were not measured consecutively. Sometimes, there were a few days or even a couple of weeks of idle time between measurements. Because of this, consideration was taken so that the cycles of each interval were measured within a short time distance of each other, which was set to a maximum of two days. This was a precaution as to not attempt to fit parameters to sets of data that might carry different characteristics, given that batteries undergo aging regardless of whether they are in use or not.

To validate the results, voltage response tests were performed on the parameterized ECMs. This was done by using the measurement current as input to the ECM equations then studying the output voltage, and later comparing it to the actual measured voltage. The standard ECM model equations were used:

$$\dot{V}_1(t) = -\frac{V_1(t)}{R_1 C_1} + \frac{i(t)}{C_1}, \quad (4.1)$$

$$V_t(t) = OCV(t) - R_i i(t) - V_1(t). \quad (4.2)$$

Coulomb counting was performed for every new measured current, and based on that an OCV value was interpolated. These equations were then discretized using zero-order hold, and the stepsize was chosen to the average sampling time from the data that was used during the parameterization of the ECM. Lastly, to have some way of quantifying the performance of the ECM, aside from visually, the root mean squared error was calculated from the measured and simulated voltage:

$$RMSE = \sqrt{\frac{1}{n} \sum_{i=1}^n (V_i^t - \hat{V}_i^t)^2} \quad (4.3)$$

where,  $n$  is the total number of data points used,  $V_i^t$  and  $\hat{V}_i^t$  are the measured and simulated voltage respectively. Further on, to validate the estimated SOH, the estimated internal resistance was transformed into a measure of health according to the following equation:

$$SOH_R = 1 - \frac{R_i - R_i^{BOL}}{R_i^{BOL}}. \quad (4.4)$$

This was then compared with the capacity measurements provided by NASA, which in turn were converted to a state of health via the following:

$$SOH_C = 1 - \frac{C_{BOL} - C_{nom}}{0.2C_{BOL}}. \quad (4.5)$$

This, as previously explained, gave the SOH in a range of 1 through 0. However, since NASA had used the batteries beyond their recommended EOL, to study the effect of overuse, this health measure thus passed zero and entered a negative domain.

## 4.1 BRLS results

The batch-wise RLS converged and consistently provided values in roughly the same range for multiple batteries. The estimated ECM parameters derived from all five intervals of battery #5 are shown in Figure 4.1. The rest of the ECM parameters for battery #6, #7, and #18 are found in the appendix in Figures 7.1, 7.2, and 7.3. The corresponding voltage response test for one set of parameter values for battery #5 can be seen in Figure 4.2. Similar voltage response tests for the rest of the batteries are found in the appendix in Figures 7.4, 7.5, and 7.6. Since the capacitance was scaled by the sampling time in the conversion from estimates to ECM parameters, the value would not converge given that the sampling time varied. To resolve this, the algorithm used the average sampling time for each cycle. Each interval consisted of 20 cycles, but it can be noted that some intervals contained a lot fewer batches. This was due to the uneven size

of the cycles due to the uneven sampling time and the time one cycle took to measure.

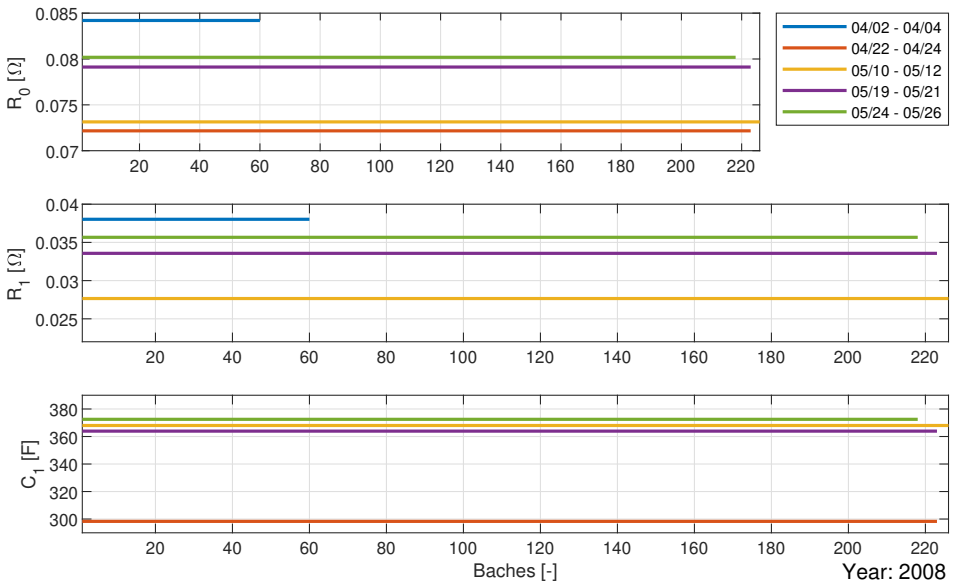


**Figure 4.1:** Parameterization results for five intervals from battery #5. Note that some values are too large to fit in the frame.

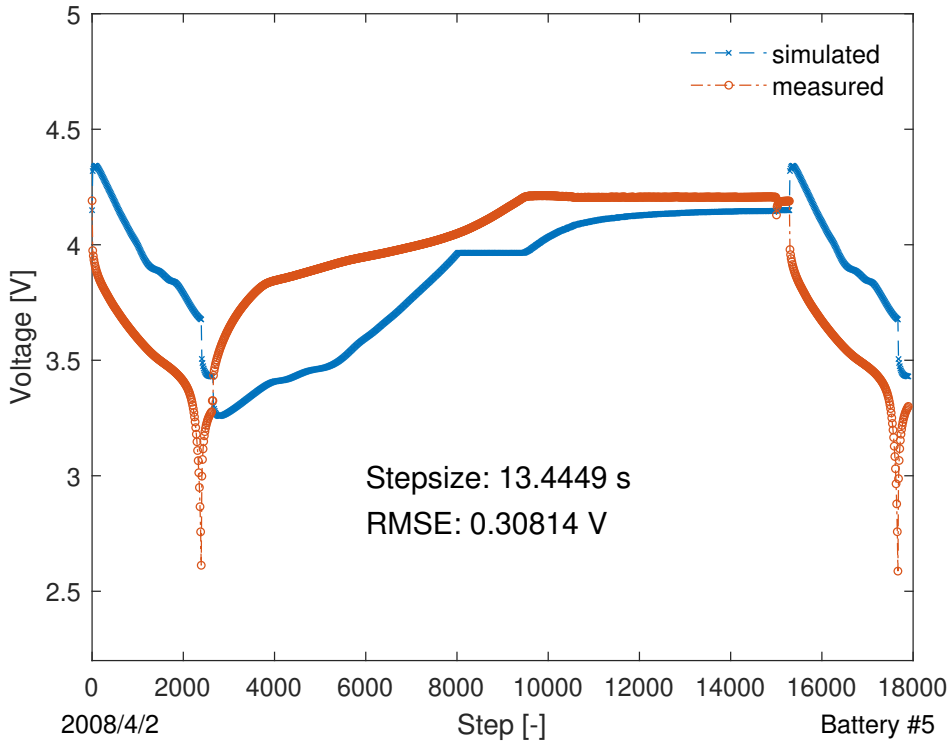


**Figure 4.2:** Simulated voltage response, compared to observed voltage, using the ECM parameters from the first interval in Figure 4.1.

## 4.2 FFRLS results

The forgetting factor recursive least squares filter performed unreliably. Sometimes the filter generated reasonable values that gave a good simulated voltage response, like in Figure 4.3 and 4.4. The sole anomaly being that the RC components turned negative; however, this turned out to be acceptable as the negative values effectively cancel each other out in the computation of the time constant for the state space model. However, when parameterizing the ECMs using different data intervals from the same battery, the resulting parameter values became illogical, leading to their inability to accurately replicate the observed voltage data in the simulation tests.

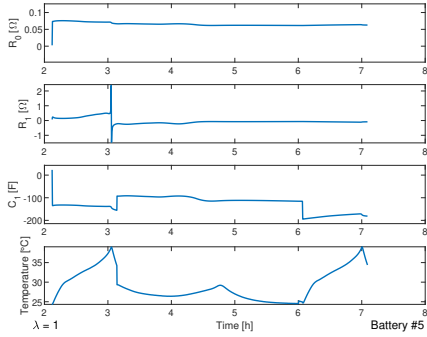


**Figure 4.3:** The parameterization results for battery #5 using the FFRLS. Temperature is added below the results, revealing a strong correlation between sharp temperature changes and the estimates jumping.

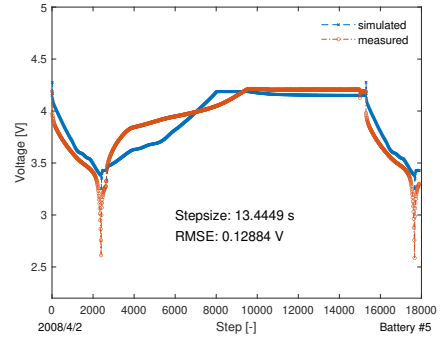


**Figure 4.4:** The simulated voltage response using the estimated ECM parameters in Figure 4.3, compared to the observed voltage.

### 4.3 Kalman filter results

The results from one interval for battery #5 are shown in Figure 4.5. In addition to the estimates, temperature and current were added to the results. It can be noted that the KF struggled to estimate the SOC correctly, remaining constantly too low. When running the Kalman filters, it was observed that the estimated values of internal resistance did not stabilize at consistent levels. Instead, these values fluctuated over time within each interval, with noticeable periods of convergence. Importantly, these periods of convergence corresponded with instances when the battery's temperature stabilized, underscoring a strong correlation between the internal resistance of the battery and its temperature. There appears an inversely proportional relationship where a high temperature corresponds with a low internal resistance. Further on, The nominal capacity  $C_{nom}$ , was initialized with the capacity value provided by NASA and then kept constant by setting the corresponding process noise to zero. This approach was considered appropriate, as within a brief duration of merely three cycles, no significant change in capacity is typically anticipated. Similarly, the SOH was initialized with 1, which was then immediately corrected in the second iteration based on the nominal capacity. It was also given zero process noise to remain constant. Lastly, the process noise for the rest of the states was arbitrarily chosen so that a reasonable result was obtained.

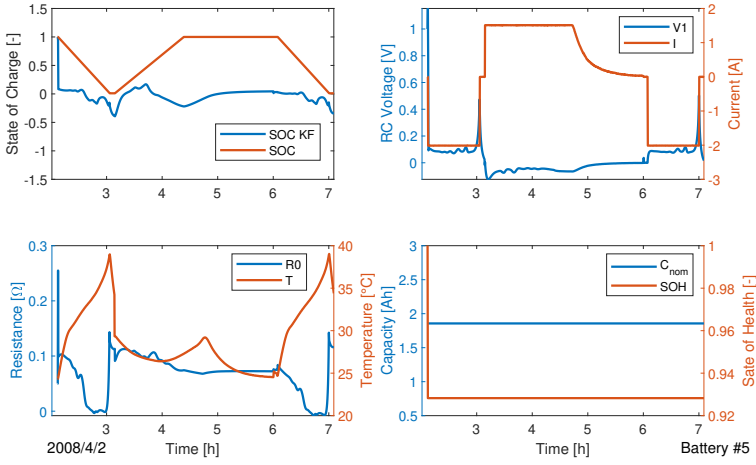


**Figure 4.5:** Kalman filter results for three cycles with added data for analysis.

## 4.4 Unscented Kalman filter results

The unscented Kalman filter, much like the standard Kalman filter struggled to accurately estimate the SOC. Similarly to the KF, the internal resistance converged when the temperature stabilized toward room temperature. It can also be noted that the internal resistance estimates decreased to negative values corresponding to high current and temperature.

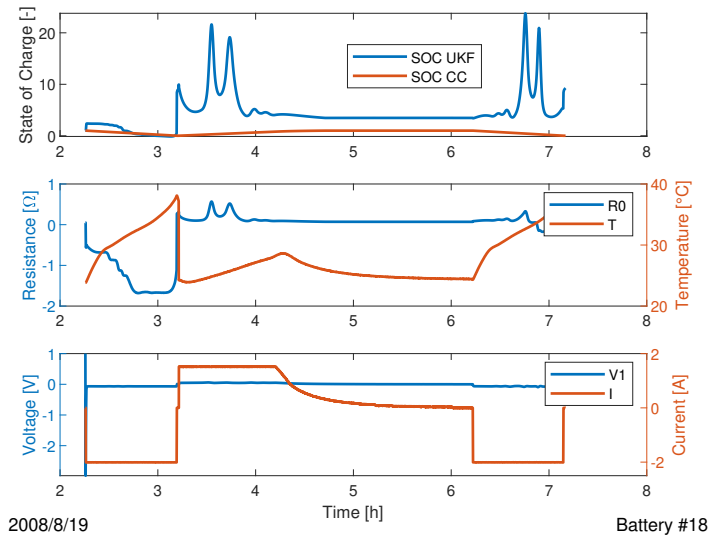


**Figure 4.6:** Unscented Kalman filter results for three cycles with added data for analysis.

## 4.5 State of health estimation

For a meaningful assessment of the state of health degradation, a single representative value of internal resistance was selected from each interval. This value was chosen at the end of the convergent sequence when the battery's temperature lies around room temperature, thus making sure that an assessment was made under similar circumstances for each interval. So in total, there were five SOH evaluations for each battery. It should be noted that even though some of the internal resistance estimates were unreasonable, such as having negative values, this did not hinder an SOH evaluation from taking place. Given the fact that there were at least some reoccurring stable parts, these were sufficient to study the relative change over time.

The results from the SOH comparison for battery #5, #6, #7, and #18 are shown in Figures 4.7, 4.8, 4.9, and 4.10. These include the KF and the UKF, as well as the results from the batch-wise recursive least squares filter. By looking at the images it becomes evident that solely relying on the parameterization of the ECM is insufficient in terms of age determining the batteries. On the other hand, the Kalman filters performed much better. The regular Kalman filter failed to capture the SOH for battery #18 but demonstrated a small degree of effectiveness in tracking the aging process in the other batteries, albeit somewhat volatile. In contrast, the unscented Kalman filter outperformed the standard Kalman filter across all batteries, staying relatively close to the true values and being less volatile.

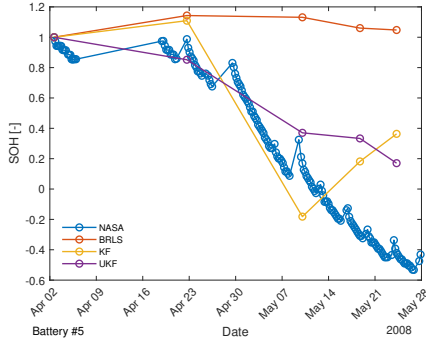


**Figure 4.7:** Battery #5 SOH degradation based on internal resistance compared to SOH degradation based on capacity.

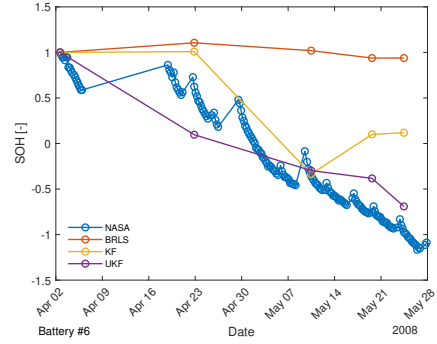


**Figure 4.8:** Battery #6 SOH degradation based on internal resistance compared to SOH degradation based on capacity.

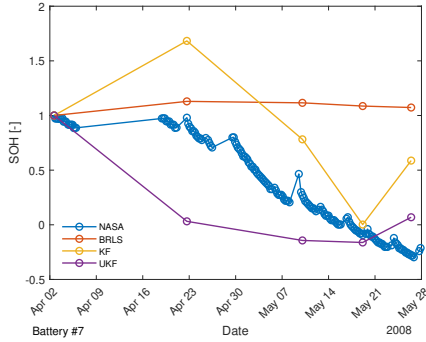


**Figure 4.9:** Battery #7 SOH degradation based on internal resistance compared to SOH degradation based on capacity.

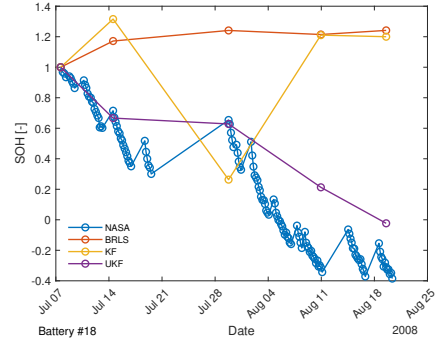


**Figure 4.10:** Battery #18 SOH degradation based on internal resistance compared to SOH degradation based on capacity.

In addition to the previously presented results, a second round of SOH comparisons was made where the measurement update for both filters was slightly redefined. Instead of using the measured voltage as a sole measurement, the difference between the voltage and the last evaluated open circuit voltage was used as a measurement. Thus redefining the open circuit voltage as  $OCV_k = OCV_{k-1} + \frac{dOCV}{dSOC}_{k-1} SOC_k$ . The results from this approach are shown in Figures 4.11, 4.12, 4.13, and 4.14. By looking at the images it is evident that the standard Kalman filter became significantly improved through this approach, while the unscented Kalman filter became significantly impaired.

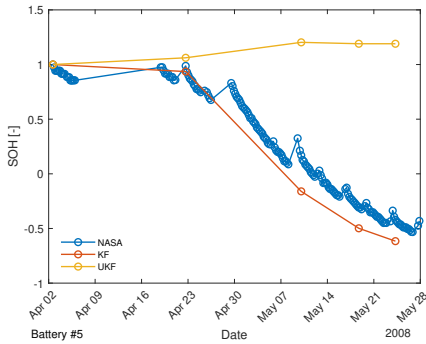


**Figure 4.11:** Battery #5 SOH degradation based on internal resistance with alternative measurement update compared to SOH degradation based on capacity.

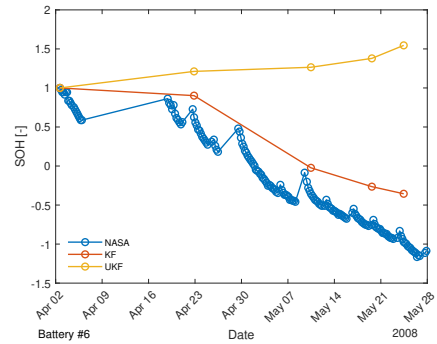


**Figure 4.12:** Battery #6 SOH degradation based on internal resistance with alternative measurement update compared to SOH degradation based on capacity.

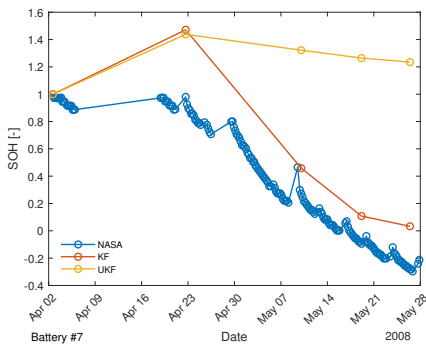


**Figure 4.13:** Battery #7 SOH degradation based on internal resistance with alternative measurement update compared to SOH degradation based on capacity.

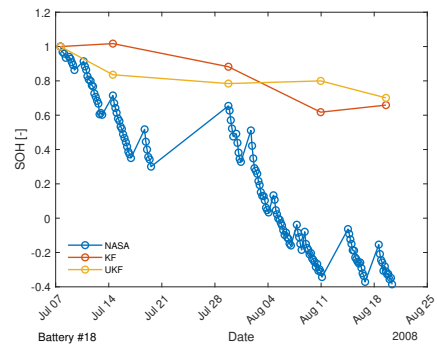


**Figure 4.14:** Battery #18 SOH degradation based on internal resistance with alternative measurement update compared to SOH degradation based on capacity.

In addition to the SOH plots, the estimated internal resistance values for the UKF and both versions of the KF are also shown in Figures 4.15, 4.16, 4.17, and 4.18. These values were used for the plots above, and the range of the resistance can be seen varying slightly between different batteries and algorithms.

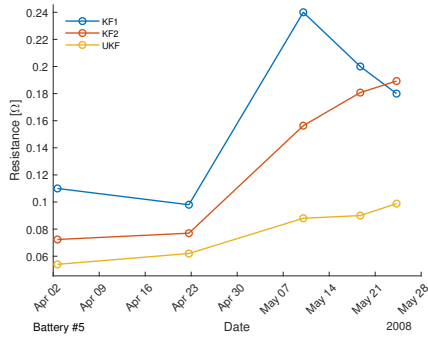


**Figure 4.15:** Internal resistance estimates for battery #5.

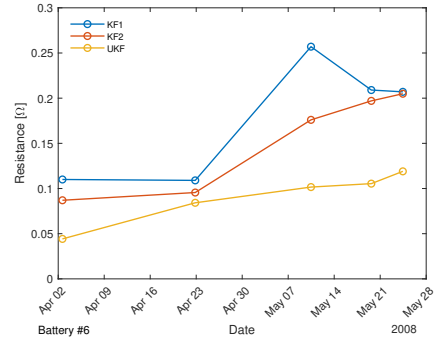


**Figure 4.16:** Internal resistance estimates for battery #6.

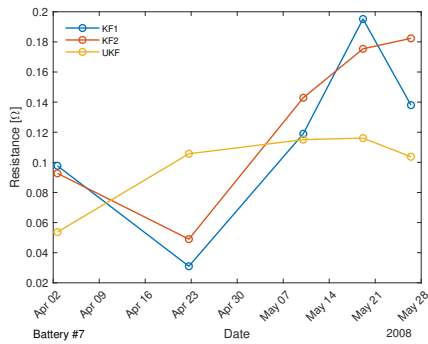


**Figure 4.17:** Internal resistance estimates for battery #7.

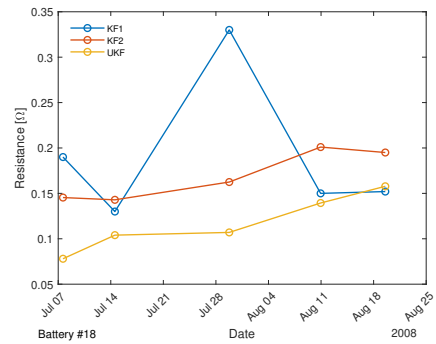


**Figure 4.18:** Internal resistance estimates for battery #18.

# 5

---

## Discussion

Under this section a discussion surrounding the results and the project at large will be made.

### 5.1 Limiting factors

There were some obstacles hindering this project. Most notably: there was no mapping between the state of charge and the open circuit voltage provided. This was a big flaw given how important the OCV is when working with ECMs. When using an ECM such as this one, there are three model parameters, as well as current, terminal voltage, and open circuit voltage. If the OCV is unknown, then there is an unknown parameter and the system of equations cannot be solved. This means that one cannot (typically) effectively parameterize the model, i.e. determine the model parameters, nor can one simulate the model, which is essentially what is done when operating a Kalman filter. Hence why knowing the OCV mapping is crucial for a successful project. Additionally, the creation of a custom OCV mapping was not possible due to the specific discharge method employed with the batteries, which hindered this possibility. To make this feasible, it would have been necessary for the batteries to undergo a gradual discharge in incremental steps. This would allow for the measurement of the Open Circuit Voltage (OCV) at each stage. Subsequently, a curve could be fitted to these OCV values in relation to the SOC. This would likely have been the ideal scenario, giving the project the highest possible accuracy to build further upon, and facilitating a more precise analysis. However, since neither option was possible, this project had to circumvent this issue by lending a pre-made OCV mapping provided by the University of Maryland for a battery with similar characteristics. However, due to the unspecified manufacturer of the batteries utilized by NASA, there remains an uncertainty regarding the accuracy of the mapping. This is especially

important given that the OCV characteristics can differ between the same type of battery manufactured by different companies. This made this a very likely source of inaccuracy, given how unique an OCV-SOC mapping can be between batteries, and how important the OCV is when working with an ECM. Another obstacle to be highlighted, is as previously mentioned, not knowing which company has manufactured the Li-ion batteries. Understanding this could have potentially unlocked numerous opportunities. For example, it would have been possible to access datasheets detailing critical specifications of the battery. These details might encompass the previously mentioned OCV-SOC table or a specified range for the expected internal resistance. Additionally, this information could extend to insights into the battery's cathode chemical composition, its physical dimensions, and the thermal characteristics of the battery materials. This would have facilitated the possibility of creating a thermal model of the battery, which could have been used in conjunction with the electrical model. Another thing that would have made the project more ideal would be if the measurement equipment had undergone analysis before the experiments began, to determine the characteristics of the measurement noise and the sensor bias. This is typically a good thing to do, as noise variance is an important piece of information in sensor fusion algorithms. As this information was not included in the data, it fell upon the user to find constant periods to perform variance measurements. It is however rather precarious to find constant voltage phases when the battery is in operation since the voltage responds the current, making it difficult to find truly constant voltage phases when the battery is in use.

## 5.2 Parameterization Challenges

Working with ECMs requires the precise determination of model parameters, a task that often proves to be non-trivial. To begin with, a design choice has to be made regarding how complex the ECM should be. This choice is a trade-off between model accuracy and model complexity, as even working with a single RC-pair ECM necessitates strenuous analytical solutions for it to be parameterized. By looking at Equation (3.15), which was used in the FFRLS algorithm, and further developing it, this becomes apparent:

$$V_t(s) - V_{oc}(s) = E(s) = -I(s) \left( \frac{R_0 + R_1 + sR_1C_1R_0}{sR_1C_1 + 1} \right), \quad (5.1)$$

$$\rightarrow \frac{-E}{I} = \frac{\frac{2}{T} \frac{1-z^{-1}}{1+z^{-1}} R_1 C_1 R_0 + R_1 + R_0}{\frac{2}{T} \frac{1-z^{-1}}{1+z^{-1}} R_1 C_1 + 1}, \quad (5.2)$$

$$\leftrightarrow \frac{-E}{I} = \frac{(2 - 2z^{-1})R_1C_1R_0 + TR_1 + TR_1z^{-1} + TR_0 + TR_0z^{-1}}{(2 - 2z^{-1})R_1C_1 + T + Tz^{-1}}, \quad (5.3)$$

$$\leftrightarrow \frac{-E}{I} = \frac{2R_1C_1R_0 + TR_1 + TR_0 + (TR_0 + TR_1 - 2R_1C_1R_0)z^{-1}}{2R_1C_1 + T + (T - 2R_1C_1)z^{-1}}. \quad (5.4)$$

This fully developed equation leads to a challenging system of equations that must be solved to gain the conversion from the estimated parameters back to ECM parameters:

$$\begin{cases} 1 = 2R_1 C_1 + T, \\ c_1 = T - 2R_1 C_1, \\ c_2 = 2R_1 C_1 R_0 + TR_1 + TR_0, \\ c_3 = TR_0 + TR_1 - 2R_1 C_1 R_0. \end{cases} \quad (5.5)$$

Successfully solving this system of equations will present a significant challenge for anyone attempting to implement these types of algorithms independently. If a double RC ECM is chosen instead, then the challenge rises to new heights, as the resulting system will contain six equations that must be solved for five parameters. This makes the methods unfeasible and the parameterization likely requires the assistance of more sophisticated software. This constitutes a drawback of the method since it is non-straightforward to implement. The challenge is further heightened when dealing with real data, as opposed to simulated data, which was the case in this project. The measurement noise was a challenging circumstance for the filters; especially for the filters that estimated the states each time a new data point was made available. This presented them with the dilemma of whether a change in the measurement data comes from the system or just the noise, and if the measurement variance is poorly evaluated the estimates can subsequently deteriorate. This was the likely cause of the failure of the FFRLS filter since it did not consider measurement noise at all. Although it could occasionally do a superior job of parametrizing a model compared to the BRLS filter, it was not sufficiently reproducible, making it an unsuitable method for noisy data. On the other hand, the BRLS filter performed much more reliably; consistently being able to generate a somewhat good model. The success can be attributed to two factors: the first is that it took into account the measurement noise and the second is that it dealt with the data in batches. Dealing with the data in batches comes with several added benefits, these include increased computational efficiency as there are fewer evaluations for the same amount of data. More so, because the evaluations are averaged out over the entire batch of data, this makes the filter less sensitive to how it has been initialized. For the same reason, it also makes the filter less sensitive to the effect of the noise, thus providing better and more reliable estimates. Regarding the limiting factors, the main disadvantage of the BRLS filter is that it did not use OCV values in the calculations. Although this was one of the aims of the method, it must still be argued that this would make the method worse than a corresponding method that does utilize the OCV. But setting this aside, the main reason why this method probably did not reach its full potential has to do with the sampling time. The authors of the original paper [14] present the method using data with a sampling time of only 0.1 seconds. This is a small enough sampling time so that the assumption of the OCV being neglectable between consecutive measurements can be upheld. The data provided by NASA on the other hand, had a much larger sampling time. The sampling time was not uniform as it varied slightly throughout a cycle, and it also varied

significantly between cycles. For example, battery #5 had an average sampling time of 9.64s for the first cycle, 18.75s for the 51st cycle, and 2.88s for the 63rd cycle. Most notably, the charge cycles generally had a lower sampling time than the discharge cycles, which is unfortunate since the discharge cycles are the most revealing when it comes to deterioration. The low sampling frequency likely hurt the estimates as the OCV assumption strayed further from being true. The uneven sampling time within a cycle also caused inaccuracy, as it necessitated using the average sampling time. This was necessary for the capacitance to converge as it was scaled by the sampling time. However, this fact probably caused an error to a lesser extent than the large sampling time.

### 5.3 Analyzing the performance of the Kalman filters

The Kalman filters did a good job of comparing the SOH for the batteries over time, showing some level of success for all batteries. However, being able to make this comparison demanded some level of ingenuity as it was not obvious at an instant how it should be made. Adding the temperature and current profiles to the plots revealed insightful information on the Kalman filter's behavior. It showed a strong relationship between the temperature and the SOC and internal resistance, thus enabling fair comparisons. However, even though the SOH comparison was successful, the performance of the individual Kalman filters was, at best, less than optimal. The SOC estimates were consistently either too high or too low. However, it should be noted that the comparison made with the SOC derived from Coulomb counting was not perfect. Coulomb counting is an imperfect and oversimplified method of estimating the SOC, and the true SOC should look much less idealized and exhibit more signs of temperature dependence. However, it still serves well as a good guiding principle for having an overall sense of where the true SOC should lie. The end of the charge and discharge cycles also served as a correction phase where the SOC was known to be either 0 or 1, thus preventing a SOC error from accumulating over time.

Regarding the internal resistance estimates, they sank too low when the battery temperature rose, being close to zero or even negative at times. This could be due to a too-strong correlation with the current, which is negative when the internal resistance estimate becomes negative for the UKF. Or, this could simply be due to inherent limitations on behalf of the filters, or inadequate tuning. However, there are still unanswered questions about how the correlation between the resistance and the temperature works, and whether the resistance profile is reasonable. For instance, the peaks in temperature coincide with a large current, which seems reasonable since the resistance causes energy loss in the form of temperature. However, it is puzzling why the resistance drops at the same time as this occurs. One interpretation of this is that a moderately higher temperature catalyzes chemical reactions in the battery, thus enhancing the mobility of Li-ions, which causes the resistance to drop. This contradicts the general notion that higher temperatures increase the resistance of a material. It should be kept in mind that internal resistance is a sum of multiple resistances, both material and

chemical; thus, the relationship between current, temperature, and resistance is complex and interdependent. It should also be highlighted that the specific values for internal resistance do not necessarily have to represent anything physically meaningful, and the internal resistance was not meant to be studied on a minute-to-minute or hourly basis. Instead, the supervision takes place over the entire battery life cycle, which spans several weeks. In other words, as long as the ambient factors such as current and temperature are similar, and the change over time is reasonable then a purposeful evaluation can still be made.

Overall there were several factors inhibiting the performance of the Kalman filters. Firstly there was the the model error, as shown in the voltage response test for the ECMs, they were not entirely able to reproduce the voltage profiles. The Kalman filter relies on the model equations to represent the system it is trying to estimate, and since the ECM is already a simplified model of a battery, an inaccurate one is poised to produce more errors for the KF. The ECM parameters mostly affected the RC-voltage estimates, but since the states were co-estimated via covariance, every estimate played a role in the totality. Further, the way the OCV was evaluated in the measurement updates was poorly defined. Instead of utilizing the derivative of the curve, it would have been best to interpolate a value for the given SOC estimate. However, this was difficult to achieve given how unrealistic the SOC estimates were, being negative or even as high as 20.

Another source of error could be the neglected effect of voltage hysteresis. Voltage hysteresis is a phenomenon where residual chemical reactions within the cell cause the voltage to behave differently whether the battery is charging or discharging [1]. This can cause the OCV to be slightly lower when charging compared to discharging for the same level of SOC. It is hard to tell how much of an impact this may have had, but it should be kept in mind, and in an ideal scenario the hysteresis should be modeled also, or there should be two OCV curves to extract values from.

Overall, the Kalman filter suffered as a result of the model equations being too simplistic. The internal resistance had no real model, and the SOC was largely a coulomb count. Further on, the Kalman filter suffered from a lack of measurements being able to correct the estimates. The sole voltage measurement that was utilized has only an indirect relationship with the states that were being estimated, making the correction more difficult and the performance more reliant on tuning. One might consider incorporating the SOC, calculated in parallel, as a form of virtual measurement. This approach could enhance the SOC estimation, yet it may not be sufficient since it would not introduce entirely new information to the filter. Instead, it may be regarded as the recycling of information already employed in the time and measurement update, given that the SOC represents merely a refined version of the current data. Adopting a more comprehensive battery model could potentially enhance the performance. Specifically, incorporating temperature data would introduce entirely new and critical information about the battery states to the filter. This again underlines the potential of thermal models in the scope of battery modeling given how the most easily available measurements are current, voltage, and temperature.

One such approach could be to introduce a thermal model. For instance, the

thermal model described in (2.1) could be utilized. This equation could be added to the time update while modeling the temperature as an additional state. The available temperature measurements could then be used in the measurement update to refine the temperature estimate, resulting in the following system of non-linear equations:

$$\dot{\hat{x}} = \begin{bmatrix} \dot{\widehat{SOC}} \\ \dot{\widehat{T}} \\ \dot{\widehat{R}}_0 \\ \dot{\widehat{V}}_1 \end{bmatrix} = \begin{bmatrix} \widehat{SOC} + \frac{\eta I T_s}{3600 C_{nom}} \\ \frac{I(OCV(\widehat{SOC}) - V)}{mc} - \frac{hA}{mc}(\widehat{T} - T_{amb}) \\ \widehat{R}_0 \\ \widehat{V}_1 e^{\frac{-T_s}{R_1 C_1}} + R_1 I(1 - e^{\frac{-T_s}{R_1 C_1}}) \end{bmatrix} + v, \quad (5.6)$$

$$y = \begin{bmatrix} V \\ T \end{bmatrix} = \begin{bmatrix} OCV(\widehat{SOC}) - \widehat{V}_1 - I\widehat{R}_0 \\ \widehat{T} \end{bmatrix} + e. \quad (5.7)$$

However, within the framework of this project, such an endeavor would have been challenging, as it would necessitate knowing the thermal properties and the weight and surface area of the battery. Out of  $m$ ,  $c$ ,  $A$ ,  $h$ , and  $T_{amb}$ , only  $T_{amb}$  is known. Therefore, the other parameters would need to be determined through an appropriate method.

Within the context of this project, internal impedance measurements were also available; however, this may not accurately represent real-world conditions. However, for the sake of exploration, one could consider using these measurements. By incorporating an extra measurement during the update phase when available, valuable insights into the internal resistance could be gained. The Kalman filter might have to be run over a larger set of cycles for this to be meaningful since the impedance measurements only are available in between cycles. The user would also have to deal with the task of deciding how these measurements can be best utilized as the EIS frequency sweep is carried out with an alternating current rather than a direct current, so there are multiple complex values for different frequencies. The results from the first and last impedance measurements can be seen in Figures 5.1 and 5.2. In the images, it is observable that the majority cluster is somewhat moved further out on the real axis. However, when considering impedance as an indicator of health, it is less consistent compared to capacity, which was the guiding parameter used by NASA. In this project, they merely served as a sanity check for the range of the internal resistance to lie within, and by comparing these impedance measurements with the internal resistance estimates in Figures 4.15, 4.16, 4.17, and 4.18 one can see that the range of the estimates was reasonable.

Lastly, one thing to consider is that the Kalman filters were initialized with the nominal capacity provided by NASA, and later updated after the discharge cycles. For the sake of purity, the update of the capacity could have been omitted, but this would likely have minimal impact, as the update is somewhat redundant, considering the small changes it brings in such a brief period. In a more realistic scenario, these values would also need to be estimated or derived through some means. A potentially beneficial approach for this project could have involved integrating the current during discharge and subsequently updating the

nominal capacity. If the capacity is part of the state vector, like the KF, then the filter would become asynchronous as the capacity unlike the other states is only updated at the end of a discharge cycle. If the capacity is instead only included in the model matrices, like the UKF, then this operation could be carried out in parallel with the filter, thus preventing the filter from being asynchronous. The success of this approach is dependent upon the dataset used. For instance, it might be effective for datasets where the battery consistently reaches full discharge, as seen with this dataset. However, in scenarios with more complex charging/discharging patterns, determining the nominal capacity becomes more challenging due to the variation introduced by partial discharges. This project did not pursue this approach due to its scope and time constraints.

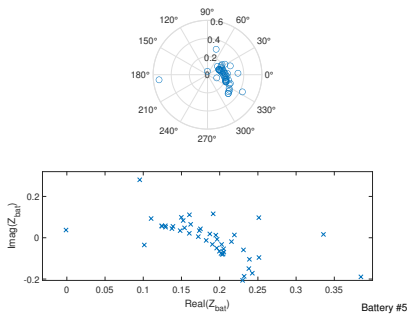


**Figure 5.1:** Battery impedance at BOL shown in a polar plot and a scatter plot.

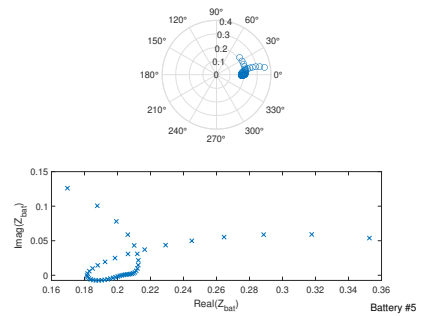


**Figure 5.2:** Battery impedance at EOL shown in a polar plot and a scatter plot.

Regarding the performance of the KF versus the UKF, the filters both worked better under different circumstances. Overall they were almost on par with each other when considering the SOH comparisons. The UKF performed superior in the original version, while the KF's performance was better when using the updated measurement equation, providing the overall best performance. The UKF is praised for its ability to handle non-linearity, something the standard Kalman filter is not designed for. Thus the reason for the UKF to perform better in the first attempt could be due to it being suited to handle the nonlinear behavior of the modeled system. This does not however explain why it failed on the second attempt, and finding a compelling reason is hard. It could be that it needs better tuning, or that not enough consideration was taken to how the estimated measurement is derived and not adjusting it too. However, due to the success of the KF, this was not given much consideration. A small drawback with the UKF is that they are a bit trickier to set up, and there is more tuning required since the spread of the sigma points also has to be tuned. In this project,  $\alpha$  had to be raised to 20 for the filter to become numerically stable, which is unusually high.

## 5.4 Reflections on Study Aims

To conclude this discussion some direct answers shall be given to the initially posed research questions. Regarding the first question, there are as previously mentioned chemical, electrical, thermal, and coupled models of Li-ion batteries. These aim to create a model with more or less fidelity depending on the use case.

The most complex chemical models are useful for advanced research on battery development analysis. They can be used to study the diffusion of Li-ions and to study the evolution of irreversible chemical reactions such as SEI layer formation, lithium plating, etc. They ultimately serve to gain a deep understanding of the nature of batteries, and where the computational load is irrelevant. However, the burdensome partial differential equations make them unsuitable for any real-time application.

In other scenarios, the computational load and time might be relevant, and thus the chemical models are redundant. A less accurate but faster model such as the electric or thermal model thus presents itself as a viable option. For instance in a work like this, or for a real-time application like a battery management system, where there are computational limitations. If the goal is to manage the heat generation and dissipation of a battery pack, then a thermal model is the most suitable. If the goal is to study the battery's behavior under different load conditions, then an electric model is most suitable. Sometimes the goal is to manage both temperature and state of charge, then the most sensible option is a coupled electric-thermal model.

Regarding the second question on how straightforward the methods are to implement, talking about model-based solutions put to use in this project, there are some things to consider. To begin, the methods cannot be up and running without some foundation being laid. Certain things like a SOC-OCV mapping must be available or be made available, and some strategy for how the nominal capacity should be decided is needed. For thermal models, thermal properties are also needed. But if a good foundation is made available, then the methods are rather straightforward to implement. A contradiction could be a complex ECM, but this can be rounded by using ready-made tools that can parameterize these.

Regarding the third question, there can be great differences in model complexity and accuracy. Within each model domain, there exists a plethora of alternatives to choose from. For example, ECMs can be made extremely simplistic by omitting the RC component and only having a resistor or made more sophisticated by adding five RC components and a hysteresis component. It all depends on how high fidelity is needed, and in this project, a classic Thevenin model was deemed sufficient based on research. The same goes for thermal and chemical models, as several model choices can be made. A challenge with parameterizing a model is, for example, the quality of the data. If the sampling frequency is too low or if the data is too noisy, the parameterization can become poor. The complexity can also be an obstacle if tough analytical solutions are needed.

Lastly, one might consider how a model-driven approach compares to a data-driven approach; for this, several points must be made. To begin with, completely

circumventing setting up a model can be a great relief as merely creating and obtaining a functioning model is an intricate art. Elmahallawy et al [3] showed great results in SOH estimation using a double-layered artificial neural network by training the algorithm using sequences of voltage and temperature profiles. This approach should be considered a more direct method of estimating SOH, by excluding some otherwise redundant work.

Apart from assessing the general health of batteries, an important area of research in diagnostics is fault isolation, which often involves reasoning deductively to find which fault mode gives rise to faulty behavior. This goes further than detecting behavior that deviates from nominal operations. Here, both model-based and data-driven approaches can be powerful tools, but both have their respective shortcomings. A general problem with data-driven models is that they require large sets of data to train the algorithms, something that is not always readily available. This inaccessibility is exacerbated when the algorithms require training with faulty data, such as when performing fault isolation. With model-based approaches comes the ability to model individual faults together with other parameters, as shown by Liu et al in [9], where a thermal and electrical model is created and several fault modes are modeled. Here the challenge is to have a well enough parameterized model for the method to work well, something that can be difficult as shown in this work. Still, model-driven approaches are a powerful tool in battery diagnostics and will not fall out of fashion since the lack of faulty data limits the potential of data-driven approaches.



# 6

---

## Conclusions and Future Work

### 6.1 Conclusion

The objective of this work was to evaluate a model-based approach for the diagnostics of lithium-ion batteries. Specifically, it aimed to assess how effectively a model could be parameterized using real-world data in conjunction with sensor fusion algorithms to estimate battery health. To summarize the results, it was possible to parameterize the ECMs using recursive least-squares filters, albeit not perfectly; despite the absence of critical elements, such as an OCV-SOC mapping. The failure of the FFRLS filter is largely attributed to it not being designed to handle noisy data, which made it an unsuitable method for this work. Conversely, the BRLS filter's relative success is attributed to it incorporating noise variance and mitigating numerical instability by processing the data in batches.

Further on, the Kalman filters struggled to accurately estimate the SOC, although the consequences of this were lesser than expected. At the same time, the Kalman filters were successfully used to observe the increase in internal resistance throughout the life cycle of the batteries, which could be rendered in SOH graphs that to varying degrees succeeded in replicating the corresponding ones provided by NASA. The partial success of the Kalman filter can be attributed to sufficiently parameterized models and adequate tuning.

The findings of the project reflect both the potential of adaptive filtering as a tool in model-based diagnostics and the challenges in using these methods with real data. The choice to use equivalent circuit models was based on their prevalence in battery diagnostics, and their relative ability to capture key dynamic behavior, despite their simplicity. The use of the least squares filters was motivated by the desire to study how adaptive filters could be used to parameterize models. Lastly, the Kalman filters were chosen for their renowned ability to process data and refine estimates in real time.

Regarding the restrictive conditions that limited the outcome, much can be summarized as an accumulation of errors at the sub-steps leading up to the final results. The lack of a more covering model entailed certain inaccuracies, which were further exacerbated by the shortcomings of the parameterization. As well as the simplistic way of evaluating the SOC, and the inept OCV mapping led to further errors. From a diagnosis perspective, it can be mentioned that there was a general lack of redundancy, both in terms of hardware and models. Meaning there were few measurements to reveal the state of the system, and a lack of simple enough model equations to accurately describe the evolution of the states. Despite this, the sensor fusion algorithms and ECMs still proved to be powerful tools being able with adequate supervision to provide worthwhile results.

In conclusion, because Li-ion batteries are chemical storage units, they are inherently difficult to model as they exhibit nonlinear and dynamic behavior; the system changes over time, with usage, and as a result of environmental circumstances, and many important parameters are interdependent and nonmeasurable. Yet these facts, together with Li-ion batteries' surge in prominence, are what makes battery diagnostics and modeling an intriguing field of research, one that is highly interdisciplinary by nature.

## 6.2 Future work

As Per future work, it would be interesting put focus on achieving a thermal model that can be coupled with the already working ECMs. The thermal model does not need to be complex at the start, as it can be further developed later, and the same goes for the ECM. This could then be used in an unscented Kalman filter, or even more interesting in a particle filter that can handle non-linear and non-Gaussian systems. The UKF can also be further advanced by putting it in a square root form which could make it more numerically stable. It could also be possible to model the nominal capacity and add it as a state. It would also be interesting to create more advanced ECMs with more RC-pairs, or with slightly different wiring. There are many options to choose from, and one could try and utilize the curve-fitting toolbox in MATLAB for parameterization. Lastly, the promising results from handling the data in batches would make it interesting to try and implement it in a Kalman filter.

# 7

---

## Appendix

### 7.1 Result from ECM parameterization and validation

Below are some pictures from the parameterization of the ECM with BRLS for batteries #6,#7, and #8, shown in Figures 7.1, 7.2, and 7.3 respectively. In addition, the corresponding corresponding voltage response tests are shown in Figures 7.4, 7.5, and 7.6.

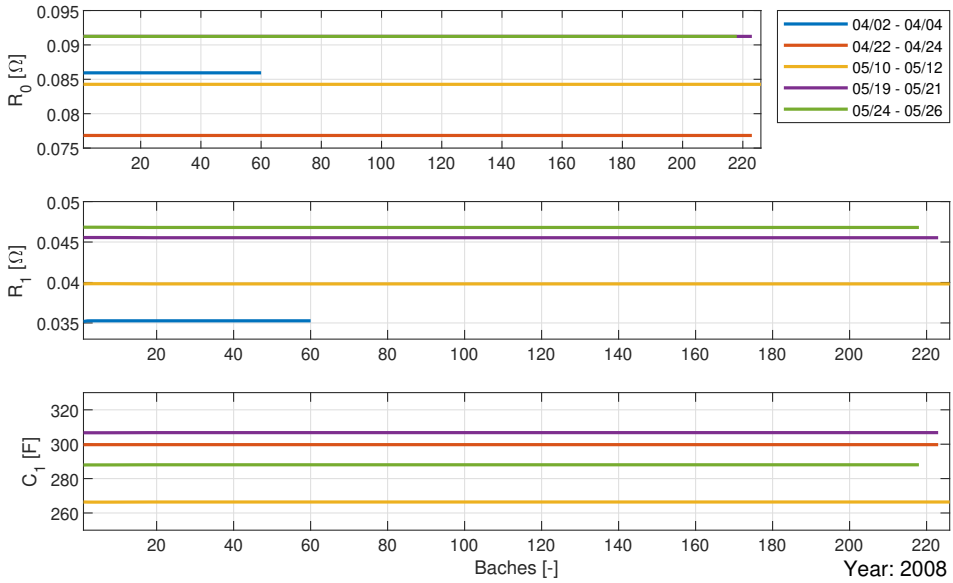


**Figure 7.1:** Parameterization results for five intervals from battery #6. Note that some values are too large to fit in the frame.

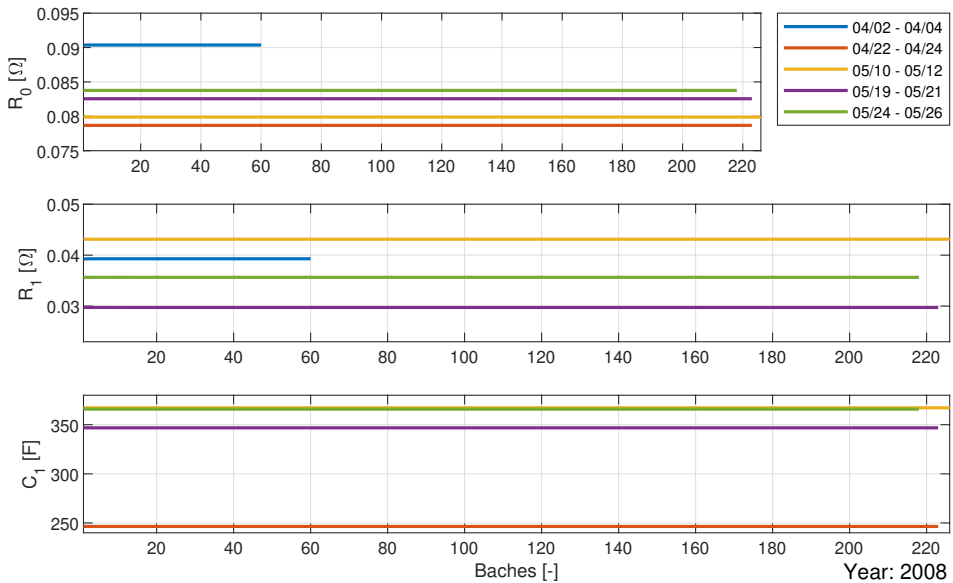


**Figure 7.2:** Parameterization results for five intervals from battery #7. Note that some values are too large to fit in the frame.

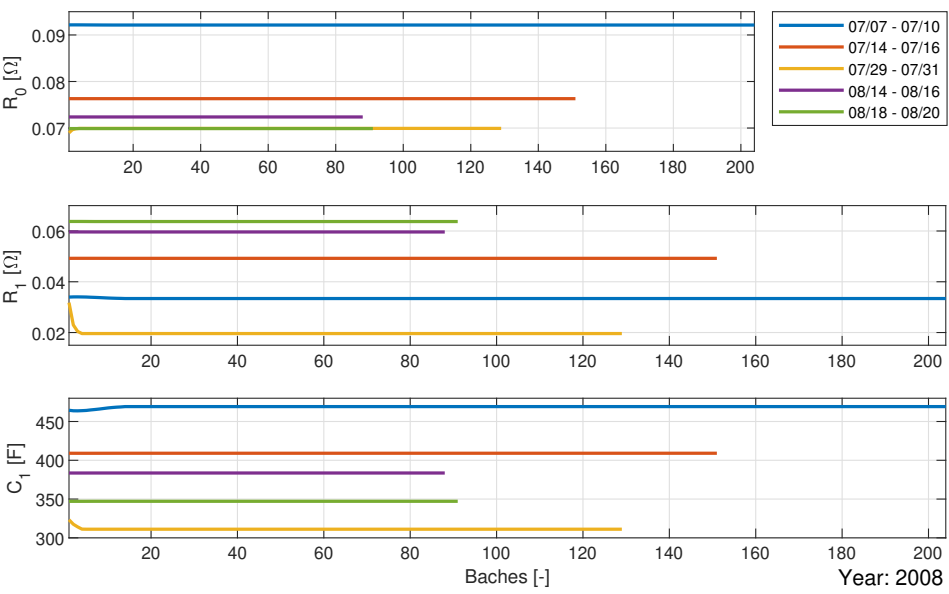


**Figure 7.3:** Parameterization results for five intervals from battery #18. Note that some values are too large to fit in the frame.

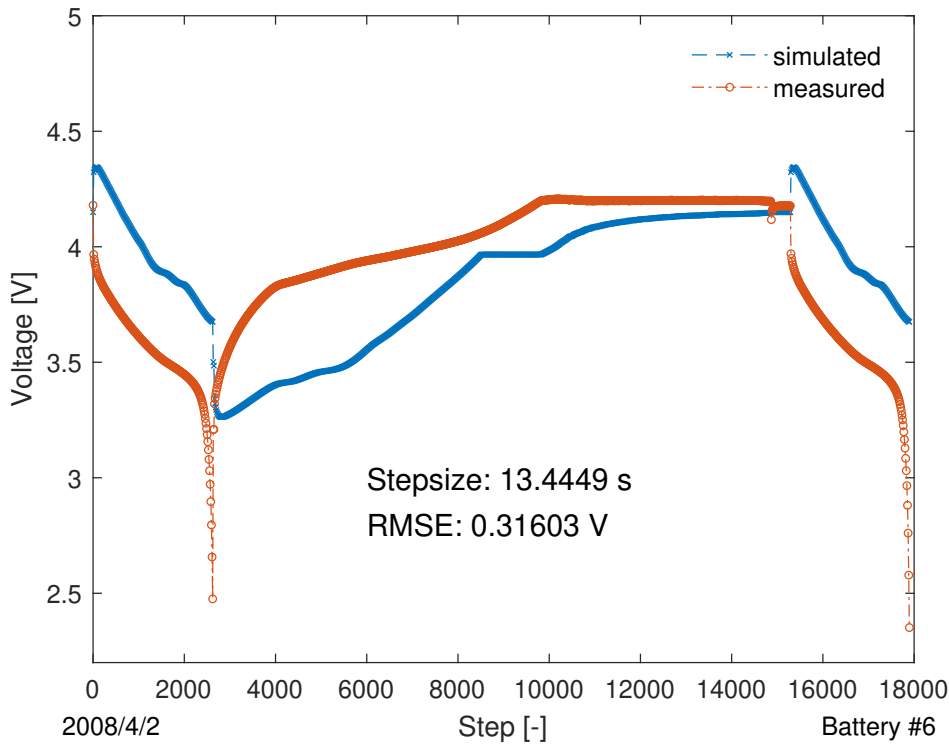


**Figure 7.4:** Simulated voltage response, compared to observed voltage, using the ECM parameters from the first interval in Figure 7.1.

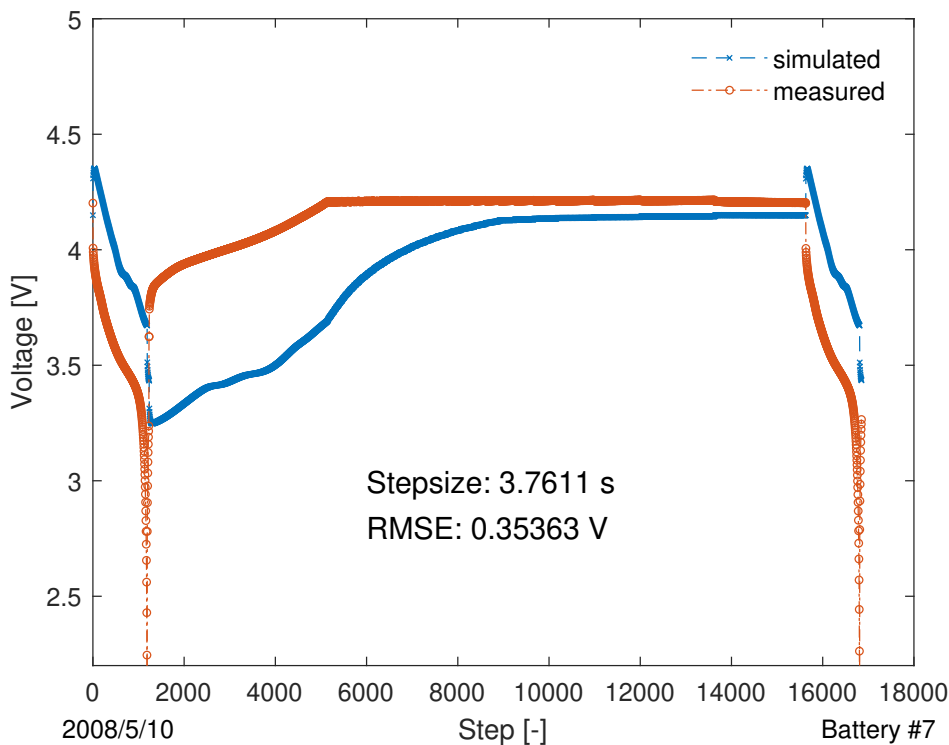


**Figure 7.5:** Simulated voltage response, compared to observed voltage, using the ECM parameters from the third interval in Figure 7.2.

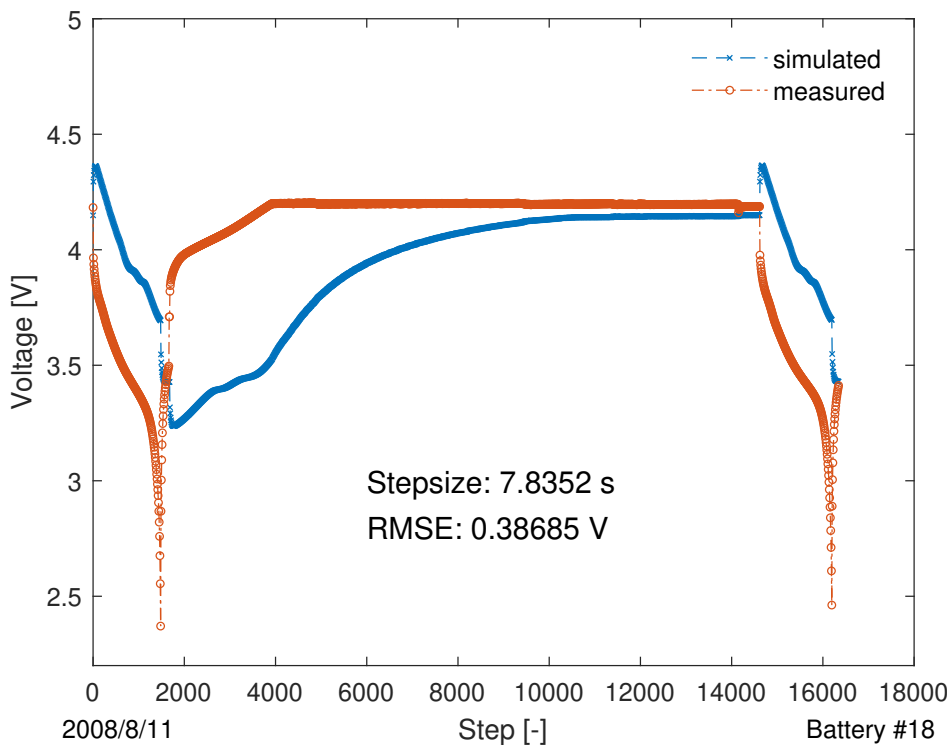


**Figure 7.6:** Simulated voltage response, compared to observed voltage, using the ECM parameters from the fourth interval in Figure 7.3.

---

## Bibliography

- [1] Helena Berg. *Batteries for Electric Vehicles, Materials and Electrochemistry*. Cambridge University Press, 2015. ISBN 9781316090978. doi: <https://doi.org/10.1017/CBO9781316090978>.
- [2] Erich Fleming et al. NASA li-ion battery aging datasets. [https://data.nasa.gov/dataset/Li-ion-Battery-Aging-Datasets/uj5r-zjdb/about\\_data/](https://data.nasa.gov/dataset/Li-ion-Battery-Aging-Datasets/uj5r-zjdb/about_data/). Accessed: 2023-09-30.
- [3] Mohamed Elmahallawy et al. A comprehensive review of lithium-ion batteries modeling, and state of health and remaining useful lifetime prediction. *IEEE Access*, 2022. doi: 0.1109/ACCESS.2022.3221137.
- [4] Paris Ali Topan et al. State of charge (soc) and state of health (soh) estimation on lithium polymer battery via kalman filter. In *2016 2nd International Conference on Science and Technology-Computer (ICST)*, 2016. doi: 0.1109/ACCESS.2018.2854224.
- [5] Rui Xiong et al. A double-scale, particle-filtering, energy state prediction algorithm for lithium-ion batteries. *IEEE Transactions on Industrial Electronics*, 2018. doi: 10.1109/TIE.2017.2733475.
- [6] Ryan Ahmed et al. Model-based parameter identification of healthy and aged li-ion batteries for electric vehicle applications. In *SAE 2015 World Congress Exhibition*, 2015. doi: 10.4271/2015-01-0252.
- [7] Shulin Liu et al. A method for state of charge and state of health estimation of lithium-ion battery based on adaptive unscented kalman filter. In *2022 International Conference on Energy Storage Technology and Power Systems (ESPS 2022)*, 2022. doi: <https://doi.org/10.1016/j.egyr.2022.09.093>.
- [8] Xiaosong Hu et al. Advanced fault diagnosis for lithium-ion battery systems. *IEEE Industrial Electronics Magazine*, 2020. doi: 10.1109/MIE.2020.2964814.
- [9] Zhentong Liu et al. Fault detection and isolation for lithium-ion battery system using structural analysis and sequential residual generation. In

- ASME 2014 Dynamic Systems and Control Conference*, 2014. doi: 10.1115/DSCC2014-6101.
- [10] Fredrik Gustafsson. *Statistical sensor fusion*. Studentlitteratur AB, 2018. ISBN 978-91-44-12724-8.
- [11] J. Kim and B. H. Cho. State-of-charge estimation and state-of-health prediction of a li-ion degraded battery based on an ekf combined with a per-unit system. *IEEE Transactions on Vehicular Technology*, 2011. doi: 10.1109/TVT.2011.2168987.
- [12] MATLAB. Control system toolbox. <https://se.mathworks.com/products/control.html>. Accessed: 2024-02-22.
- [13] University of Maryland. Battery research data. <https://calce.umd.edu/data#INR/>. Accessed: 2023-12-06.
- [14] Sheikh Arif Raihan and Balakumar Balasingam. Recursive least square estimation approach to real-time parameter identification in li-ion batteries. In *2019 IEEE Electrical Power and Energy Conference (EPEC)*, 2019. doi: 10.1109/EPEC47565.2019.9074825.